ISBN 0-315-61828-0

SURFACE AND AIRBORNE INFRARED DETECTION OF SEA ICE HAZARDS

RICHARD DONALD WORSFOLD

SURFACE AND AIRBORNE INFRARED DETECTION OF SEA ICE HAZARDS

By

RICHARD DONALD WORSFOLD

Submitted in Partial Fulfillment
of the Requirements of M.Eng. at
Memorial University of Newfoundland.

August 21, 1981

ISBN 0-315-61828-0

ABSTRACT

This Masters Report is concerned with the assessment of the capability of instruments to detect ice hazard targets using the infrared portion of the electromagnetic spectrum. It is a target/sensor interaction study and discusses infrared theory, atmospherics, basic infrared systems and the targets being sensed. These factors are assessed to determine optimum infrared capability.

The results of this target/sensor interaction study shows that the temperature ranges to be sensed for sky, marine and targets are basically ambient temperature (-20^{o} to $20^{o}C$). Wavelengths for sensing are identified as the 3 to 5 micrometer and 8 to 14 micrometer ranges with a peak wavelength of 10.6 micrometers identified as the optimum for sensing the temperature range -20^{o} to $20^{o}C$.

The report shows that the potential exists to use infrared systems and devices to detect and monitor icebergs and sea ice but before conclusive detection can be achieved the ice targets such as icebergs, bergy bits, growlers, multi-year floes and first year floes must be characterized according to their

infrared signature. The lack of characteristic infrared target signatures is the weakest link in assessing the capability of any infrared sensor for ice detection. A target signature program is recommended for both wavelength ranges discussed, the 3 to 5 micrometer and the 8 to 14 micrometer.

ACKNOWLEDGEMENT

The author of this Masters Report would like to acknowledge the support of various persons and organizations for their part in the development of this document. The report is written to fulfill the requirements for a Masters in Ocean Engineering at Memorial University of Newfoundland. Academic requirements were eight (8) courses and a technical report. This program was carried out on a part time basis commencing in the fall of 1975 under the direction of the late Dr. David Dunsiger. After his death, Dr. Adam Zielinski assumed direction responsibilities. The author would like to thank both for their direction and a special thank you to Dr. Zielinski for assuming this role so late in the program.

A special thanks is extended to Dr. Surendra Parashar of REMOTEC Applications Inc. who reviewed this document before submission.

TABLE OF CONTENTS

LIST OF FIGURES

LIST OF TABLES

LIST OF SYMBOLS

A = Area of Source and Percent Absorptance

BB = Blackbody

E = Radiative Power (Wm^{-2})

K = 2897.9 micrometers ^{o}K (a constant)

K_a = Absorption Coefficient

K_1 = 3.74×10^8 (a constant)

K_2 = 1.44×10^4 (a constant)

L = Radiance

L_v = Luminance (photometric brightness)

MTF = Modulation Transfer Function

M = Radiant Exitance

M = Radiant Exitance at a Specific Wavelength

MRy = Megarayleigh, MRy corresponds to a photon radiance of $\frac{1}{4\pi} \times 10^6$ photons sec^{-1} cm^{-2} sr^{-1}

R = Percent Reflectance and Percent Transmittance

T = Temperature

T_r = Radiation Temperature

W = Watts

e = Napierian Base Exponential

g = grams

Km = Kilometers

m = meters

nm = nautical miles

Φ = Radiant Flux

α = Absorptance

ϵ = Emissivity

ϵ_λ = Spectral Emissivity

ρ = Reflectance

τ = Transmittance

θ, ϕ = Angular Measurements

σ = Stefan-Boltzmann Constant

σ_s = Roughness Factor

λ = wavelength

m = micrometer

cm = centimeters

CHAPTER 1

INTRODUCTION

1.1 General Statement

With the increase in vessel traffic and petroleum exploration activity in the ice covered waters of the Arctic and Canada's east coast, the number of ocean vessels and platforms required to work in these areas will increase in the 1980's. These areas are characterized by long periods of darkness, unstable meteorological conditions, changing sea ice cover and icebergs. For ships plying these waters navigation can be treacherous and difficult. For an exploration platform to be operated in these areas, a need to identify the hazards will be required. To attain a high degree of safety for operating in these areas a system for the recognition and identification of ice hazards is required. This system, an "ice hazard detection system" is highly complex and consists of a suite of sensors and interfaces working together to provide the information required by the vessel captain or platform operator.

Under normal circumstances, it would appear that marine radar, an all-weather sensor, would be the most

logical sensing system to use. Radars are highly developed and are used on all ships. The major problem is that marine radars have been optimized to detect and monitor other ships and not ice hazard targets. Recent data from marine radars of iceberg targets has shown that satisfactory target detection and monitoring capability is not attainable (Worsfold et al, 1979; REMOTEC, 1980, and Parashar et al, 1981). This has resulted in a number of contract and grant studies by REMOTEC Applications Inc. of St. John's, Newfoundland to assess the feasibility of radar, sonar, infrared, low light level television, laser radar, passive microwave and multispectral electro-optical sensor systems for use in an ice hazard detection system that will reliably detect and monitor ice targets.

In this report infrared radiation and sensors will be studied as a promising supplement to an ice hazard detection system. The document will cover the basic infrared theory, atmospheric conditions that will be encountered, the basic components of any infrared system and data concerning ice hazard targets.

1.2 Target/Sensor Scenario

To place this study in its proper perspective, a scenario must be developed to show how the infrared sensor will be used. It is assumed that a stationary

platform such as a drilling ship will be used for observations.

Figure 1 show the three horizons that represent the range view from a ship. The sea horizon is the geometrical horizon. It is the locus of tangency points for all straight lines and that graze the earth from the observer station. Because atmospheric refraction occurs the distance at which the horizon can be observed increases and is more distant than the geometrical or sea horizon because the light waves are bent by the index of refraction the observer can see over the "hump" or geometrically further point of observation. At radar frequencies the bending due to the index of refraction is greater than for the optical case thus the radar can "see" further over the "hump". For infrared systems the optical horizon is used.

The line of site around the drill ship can be found from Figure 1. Practical considerations limit the maximum sensor elevation above the water level to approximately 28 m. This allows for an infrared viewing radius of approximately 11 nm.

In addition to what can be seen from the surface platform, there is the potential that this platform will receive airborne support from an aircraft or helicopter flying over the observation area which can

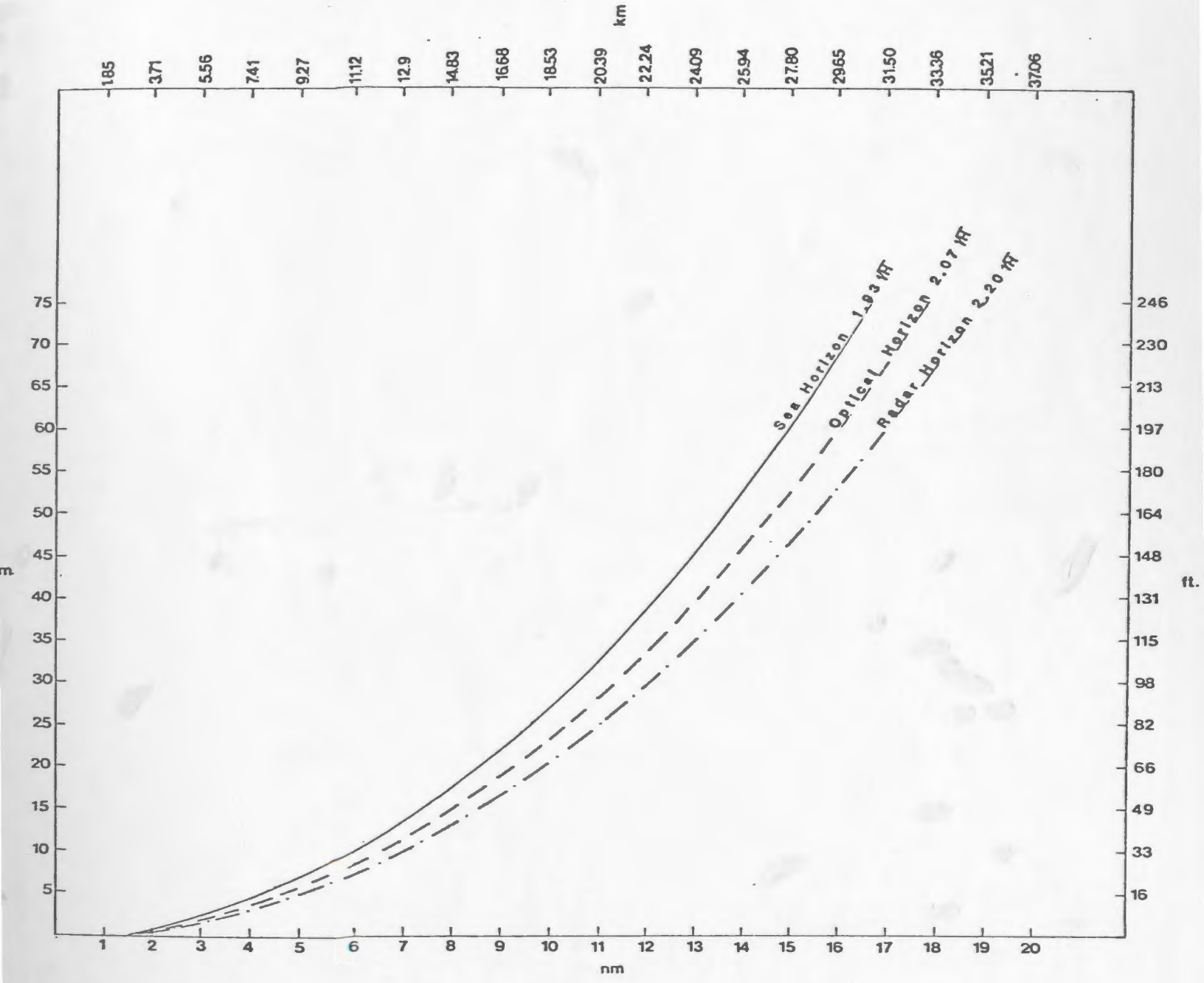

Range

Figure 1 Sea, Optical and Radar Horizons as a function of Ship's mounting height (Developed from data in Reference material)

also be equipped with infrared sensors. The normal flying altitude for remote sensing aircraft in Canada is from 1000 feet to 35,000 feet (Canada Centre for Remote Sensing, 1977). In this report support from a satellite with infrared sensors is not considered as present attainable resolution (1981) is not sufficient for ice hazard detection.

The important parameter for an infrared detection system is resolution. Growlers, bergy bits and multi-year floes can be less than five metres in size. Therefore, the sensors to be used must be capable of sensing targets of this size.

In summary, the space of operations for infrared determination of ice hazards is confined by a cylinder with 11 nautical mile radius and 6 nautical mile height. This allows for observation from the horizontal view to vertical view through a full 90^{o}. The sensor will be either on a drill platform and/or on an airborne platform. The target will be located within the full 400 square nautical mile surface area. A moving platform could be considered but will require space and time shifts for implementation. The atmospheric and oceanographic conditions within the cylinder can affect the infrared measurements. This report will discuss the use of infrared systems within this observation cylinder to determine the feasibility

CHAPTER 2

INFRARED RADIATION

2.1 Fundamentals of Infrared Radiation

This chapter is a review of the theory of infrared. Concepts discussed have been developed by a number of investigators who are referred to in the text. Major documents that summarize historical works are also given in the references. Equations are referred to by the reference from which they were taken.

Infrared instruments can detect and measure infrared radiation at considerable distances. Because of the relationship that exists between temperature and radiation, the object's temperature can be determined with a reasonable degree of accuracy from object radiation and vice versa. This can be done without physical contact and is called remote sensing or non-contact measurement.

2.1.1 Infrared Radiation

The infrared portion of the electromagnetic spectrum covers the wavelength range from about 0.75×10^{-6} meters to 1000×10^{-6} meters (Figure 2). The

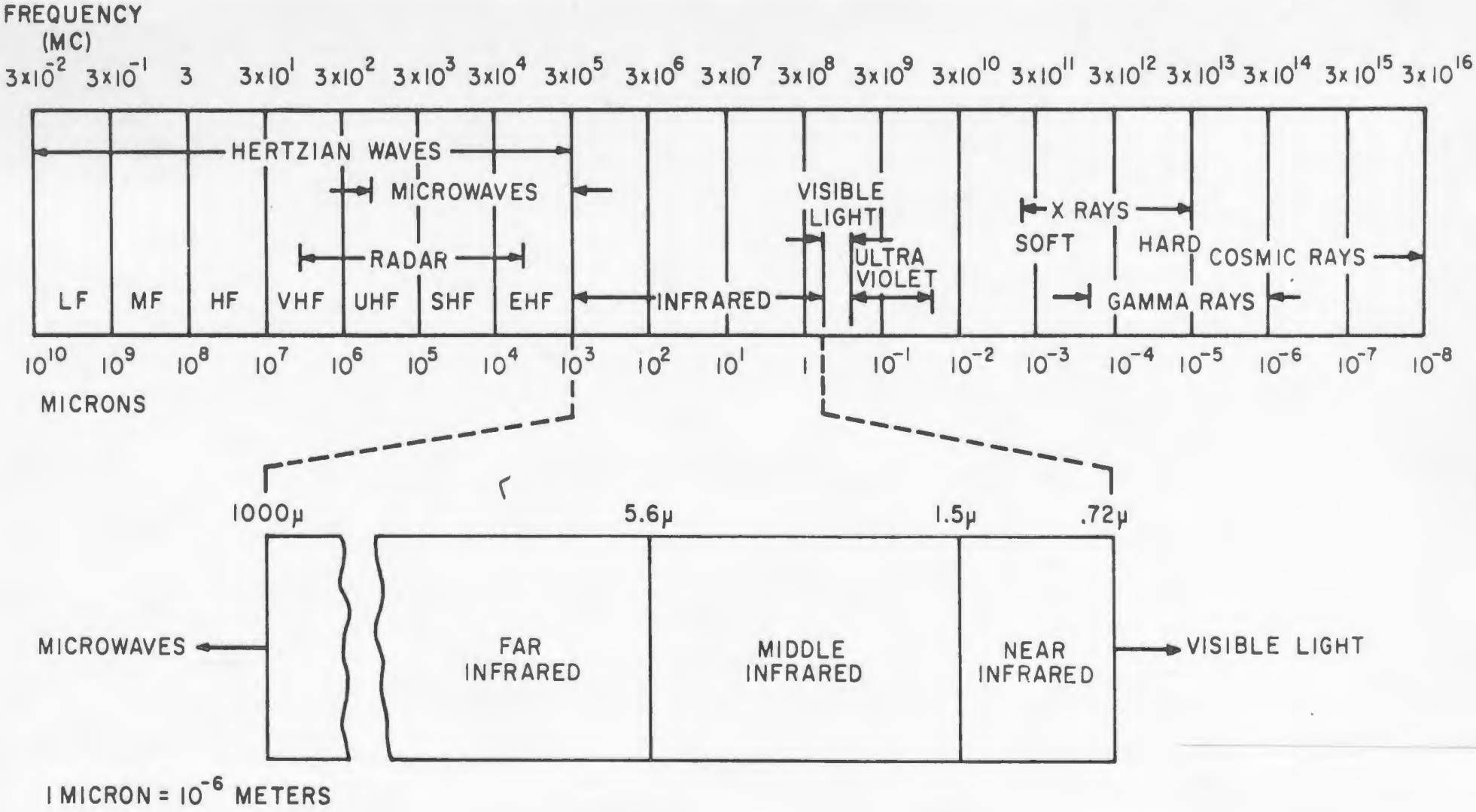

Figure 2 The location of the infrared region in the electromagnetic spectrum. (Barnes Engineering Company, 1970)

infrared range lies between the visible light range and the microwave range. The commonly used unit to describe the range is the micrometer (μm). Therefore, the infrared range is normally written as 0.75 micrometers to 1000 micrometers or 0.75μm to 1000μm.

The spectrum is customarily divided into the near infrared (0.75 to 1.5 μm), the intermediate infrared (1.5 to 5.6 μm), and the far infrared (5.6 to 1000 μm) regions.

Infrared radiation is naturally emitted by all objects with temperature above $0^{o}K$ because of the thermal agitation of the object's molecules. Radiation that is naturally emitted is called passive radiation.

The intensity, frequency and wavelength of the radiation are dependent on the temperature of the radiating source, size of the radiating source and by a property called the emissivity (ϵ) which is a characteristic of the radiating material.

When energy from a radiating source reaches another body it can be reflected by the body, transmitted through the body or absorbed and converted to heat.

The total energy reaching a body from a source object can be represented by the relationship:

$$E = T + R + A \qquad (1)$$

(Barnes Engineering Company, 1970)

where, E = total energy of object
T = object's percentage of transmittance
R = object's percentage of reflectance
A = object's percentage of absorptance

If a major part of the energy is transmitted through the object, the material is said to be transparent but if the reflectance is large the object acts like a mirror. Materials which are good transmitters or reflectors are poor emitters. Objects which readily absorb the energy are good emitters or radiators of energy. Absorption or emission of a material generally increases when the surface is roughned. Continuous absorption causes the object's temperature to increase.

2.1.2 Basic Laws

Emitted infrared energy covers a wide range of frequencies and wavelengths. The wavelength at which

the maximum or peak radiation occurs is determined by the temperature of the body (Figure 3). As the temperature increases the peak radiation shifts to shorter wavelengths and the total amount of radiated energy increases.

A standard is used in infrared studies which is called the "blackbody". A blackbody is an ideal emitter for which the total radiated energy and spectral distribution are known. To measure the relation between temperature and radiation a practical blackbody is needed which simulates the desired characteristics. A blackbody simulator and its precision temperature controller comprise a radiation reference source that links measureable temperatures and emitted radiation.

There are three basic laws which can be used to determine characteristics of target radiation.

2.1.2.1 Stefan-Boltzmann Law

This law is written as:

$$W = \epsilon \sigma A T^4 \qquad (2)$$

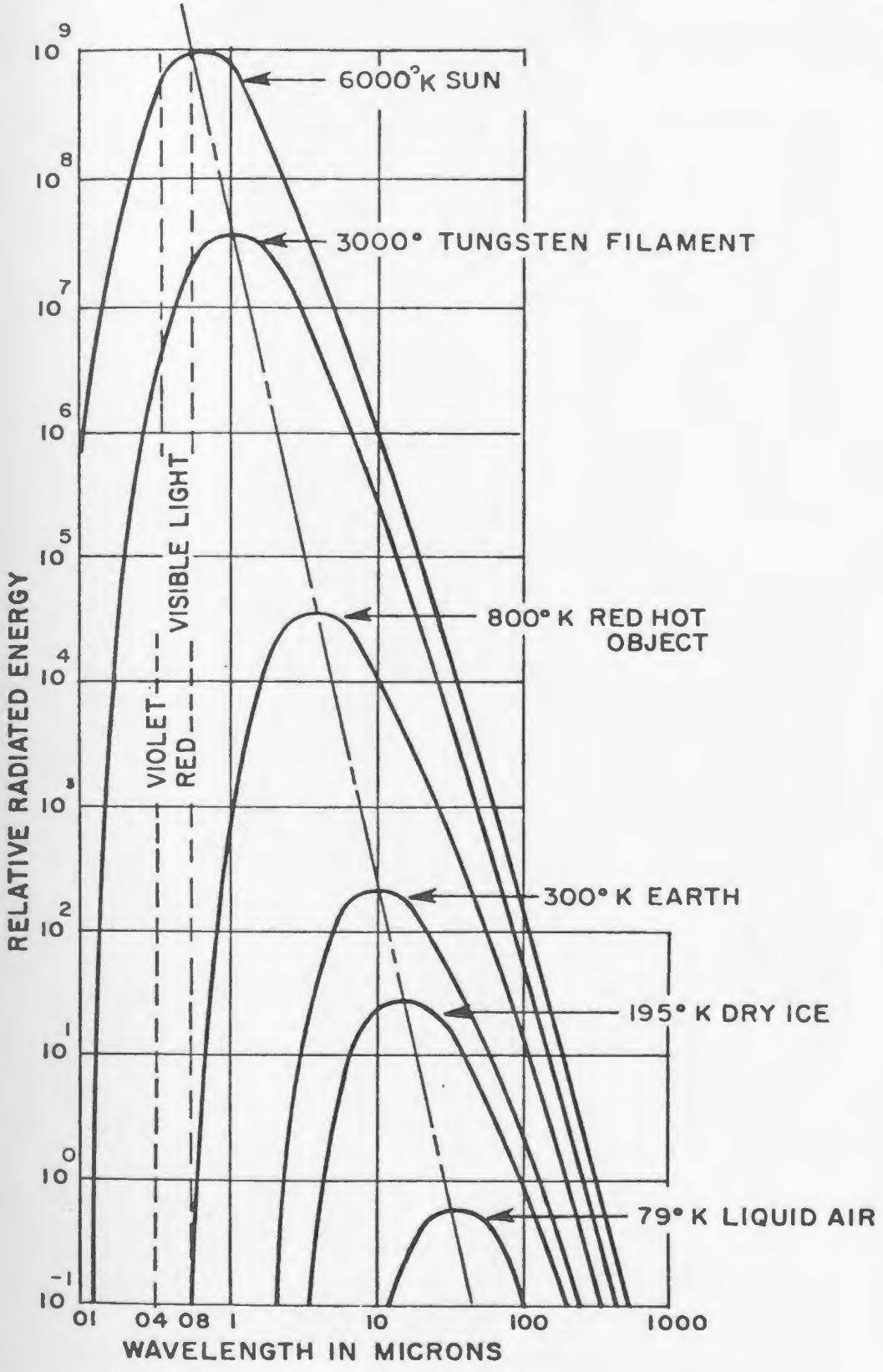

Figure 3 Spectral characteristics of blackbody radiation from objects at different temperatures. (Barnes Engineering Company, 1970)

Where, W = total radiation in watts

ϵ = emissivity

A = area of the source in centimeters squared

T = temperature of the source (^{o}K)

σ = 5.672×10^{-12} watts cm^{-2} $degrees^{-4}$ ($^{o}K^{-4}$)

(Handbook of Military Infrared Technology, 1965)

This law deals with the total radiation energy available from an object. To define ϵ, the radiation emitted by a blackbody target must be considered. Blackbody radiation is that which is emitted by an object which totally absorbs all incident radiation without any energy reflection or transmission. The radiation from the blackbody object is greater in total energy emitted than that from any other type of object at the same temperature.

Actual physical targets normally do not meet the requirements of a theoretical blackbody. The emissivity factor ϵ which is less than 1.0 is required to correct for target characteristics. Emissivity is the ratio between target radiated energy and the energy radiated by an equivalant blackbody. The value of ϵ varies with the type of material and the roughness of the target surface.

2.1.2.2 Wien's Displacement Law

All targets at temperatures above absolute zero emit electromagnetic energy over a wide band of frequencies. This energy is not distributed in equal amounts at all wavelengths corresponding to the frequency band. A maximum amount of energy is emitted at a specific wavelength. This is dependent upon the temperature and the surface characteristics of the object. The relationship is such that the wavelength of maximum energy emission becomes shorter as the temperature increases (Figure 3). Wien's Law specifies the wavelength at which maximum radiation is emitted for any specified temperature. This is stated as:

$$\lambda = K/T \qquad (3)$$

where, λ = wavelength of maximum radiation in micrometers

T = degrees Kelvin (^{o}K)

K = Wien displacement constant, 2897.9 micrometers ^{o}K

(Handbook of Military Infrared Technology, 1965)

This relationship can be used to quickly determine wavelength or temperature at maximum radiation and can

be used as a rule of thumb.

2.1.2.3 Planck's Formulations

Planck's relationships give the basic formulations of infrared theory. All other formulations such as Wien's Law can be derived from Planck's functions. These functions can be written several ways and in terms of different quantities. An example is Planck's equation for calculating emissive power in any wavelength increment:

$$E = K_1 \lambda^{-5} \left(e^{\frac{K_2}{\lambda T}} - 1\right) \qquad (4)$$

where, E is power expressed in watts cm^{-2}

$K_1 = 3.74 \times 10^8$

$K_2 = 1.44 \times 10^4$

λ = wavelength in micrometers

T = degrees Kelvin

e = Napierian base

(Infrared Handbook, 1978)

Planck's functions can be graphically presented to provide information about the spectral distribution or blackbody radiation (Figure 4). In Figure 4, M_λ is the radiant exitance at a specific wavelength. The radiant exitance is the radiant power per unit area

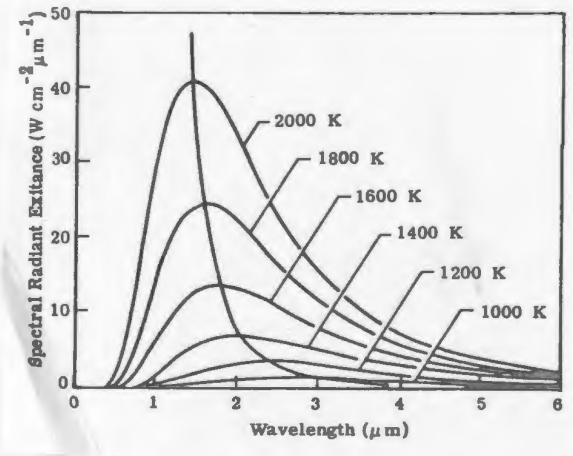

Blackbody curves, 1000 to 2000 K.

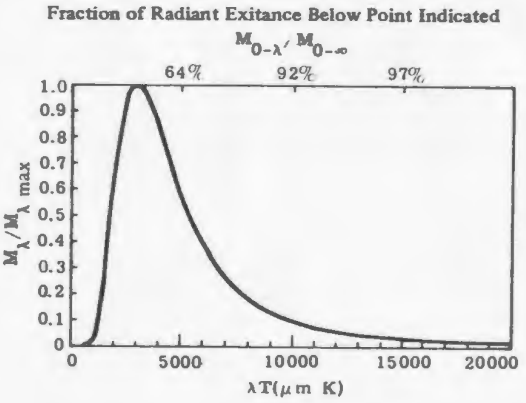

$M_\lambda/M_{\lambda_{max}}$ versus T for a blackbody.

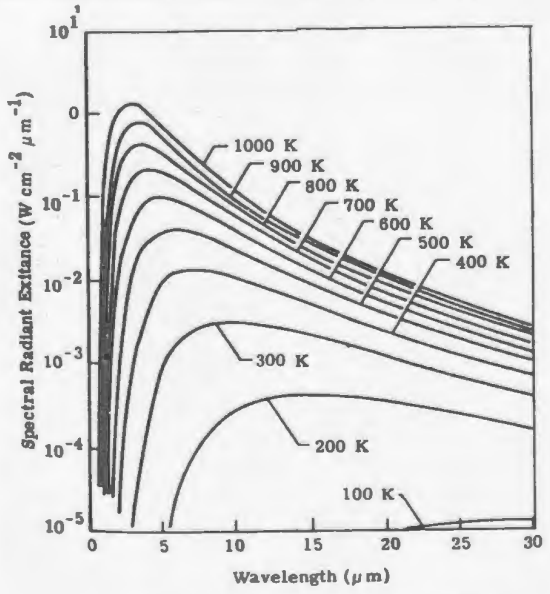

Blackbody curves, 100 to 1000 K.

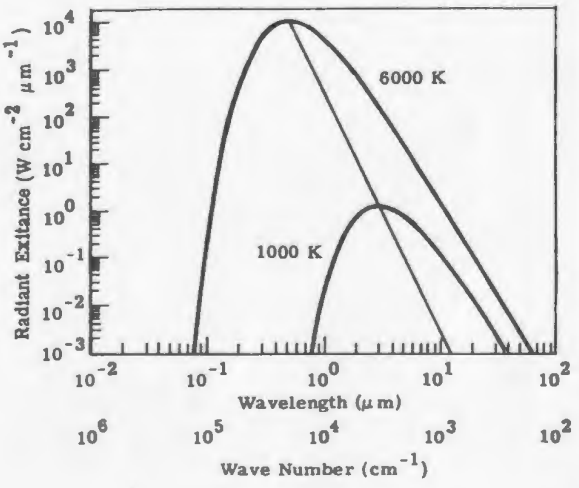

M_λ versus λ and ν.

Figure 4 Planck Curves (The Infrared Handbook, 1978)

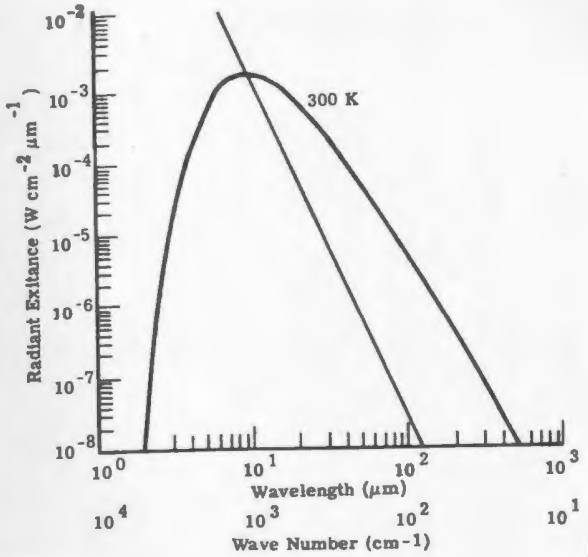

M_λ versus λ and ν.

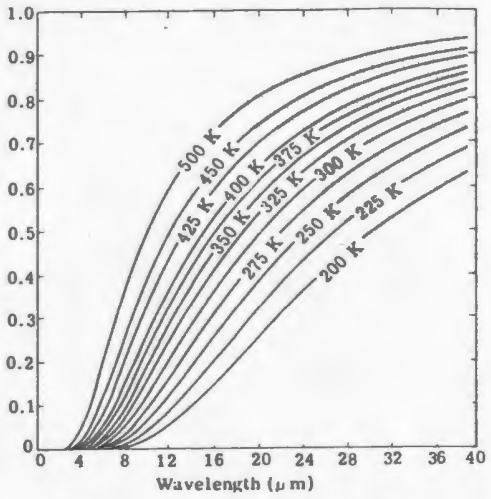

Relative photon flux density as a function of wavelength: $\int_0^\lambda M_{q,\lambda}(\lambda)d\lambda/\sigma_q T^3$.

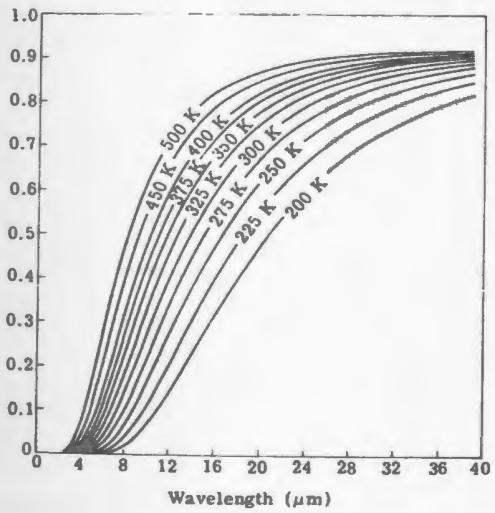

Relative radiant exitance, radiance, or radiant intensity: $\int_0^\lambda M_\lambda d\lambda/\sigma T^4$.

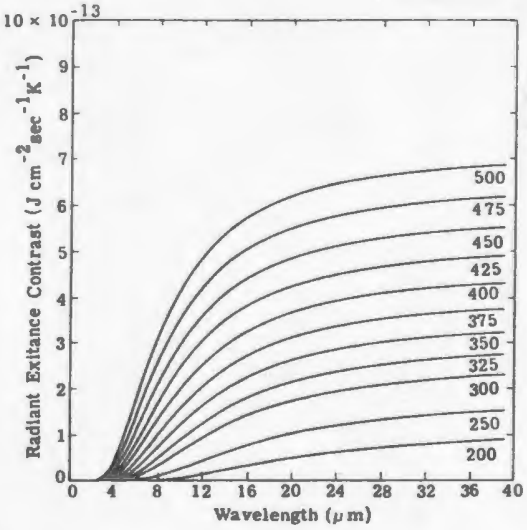

Integral of radiant exitance contrast $\int_0^\lambda \frac{\partial M_\lambda}{\partial T} d\lambda$ as a function of λ.

Figure 4 (continued) Planck Curves (The Infrared Handbook, 1978)

emitted or exiting from a surface. It can be a spectral quantity.

2.1.3 Emissivity and Related Laws

2.1.3.1 Emissivity

Emissivity is defined as the ratio of the radiant exitance or radiance at the specified wavelength of a given body to that of a blackbody. The radiance of a body is defined as the radiant power per unit solid angle per unit projected area. The defining equation for spectral emissivity is:

$$\epsilon_{\lambda} = \frac{M_{\lambda}}{M_{\lambda}^{BB}} = \frac{M_{\lambda}\ (\lambda,T)}{M_{\lambda}^{BB}\ (\lambda,T)} \qquad (5)$$

(Infrared Handbook, 1978)

where λ represents a single wavelength and T must be the same for both the numerator and the denominator. The directional spectral emissivity is the ratio of radiances (L_{λ}) and is defined as:

$$\epsilon(\lambda,\theta,\varphi) = \frac{L_{\lambda}\ (\theta,\varphi)}{L_{\lambda}^{BB}\ (\theta\ \varphi)} \qquad (6)$$

(Infrared Handbook, 1978)

Over a spectral interval the equation becomes:

$$\epsilon = \frac{\int_{\Delta\lambda} L_\lambda \, d\lambda}{\int_{\Delta\lambda} L_\lambda^{BB} \, d\lambda} = \frac{\int_{\Delta\lambda} \epsilon[\lambda] L_\lambda^{BB} d\lambda}{\int_{\Delta\lambda} L_\lambda^{BB} \, d\lambda} \qquad (7)$$

(Infrared Handbook, 1978)

and over the entire spectral band:

$$\epsilon = \frac{\int_0^\infty \epsilon[\lambda] \, L^{BB} \, d\lambda}{\pi^{-1} \, \sigma T^4} \qquad (8)$$

(Infrared Handbook, 1978)

As can be seen from equations (5) to (8) emissivity is normally defined over a certain spectral interval. Thus, there would appear to be a certain wavelength dependence. A material which has emissivity that is independent of wavelength is called a greybody. Bodies which have emissivity that varies with wavelength are called spectral bodies. Spectral bodies are sometimes referred to as coloured bodies with the signifiance of the word colour only to devote that it is not blackbody. Figure 5 shows a simplified spectral relationship for ϵ .

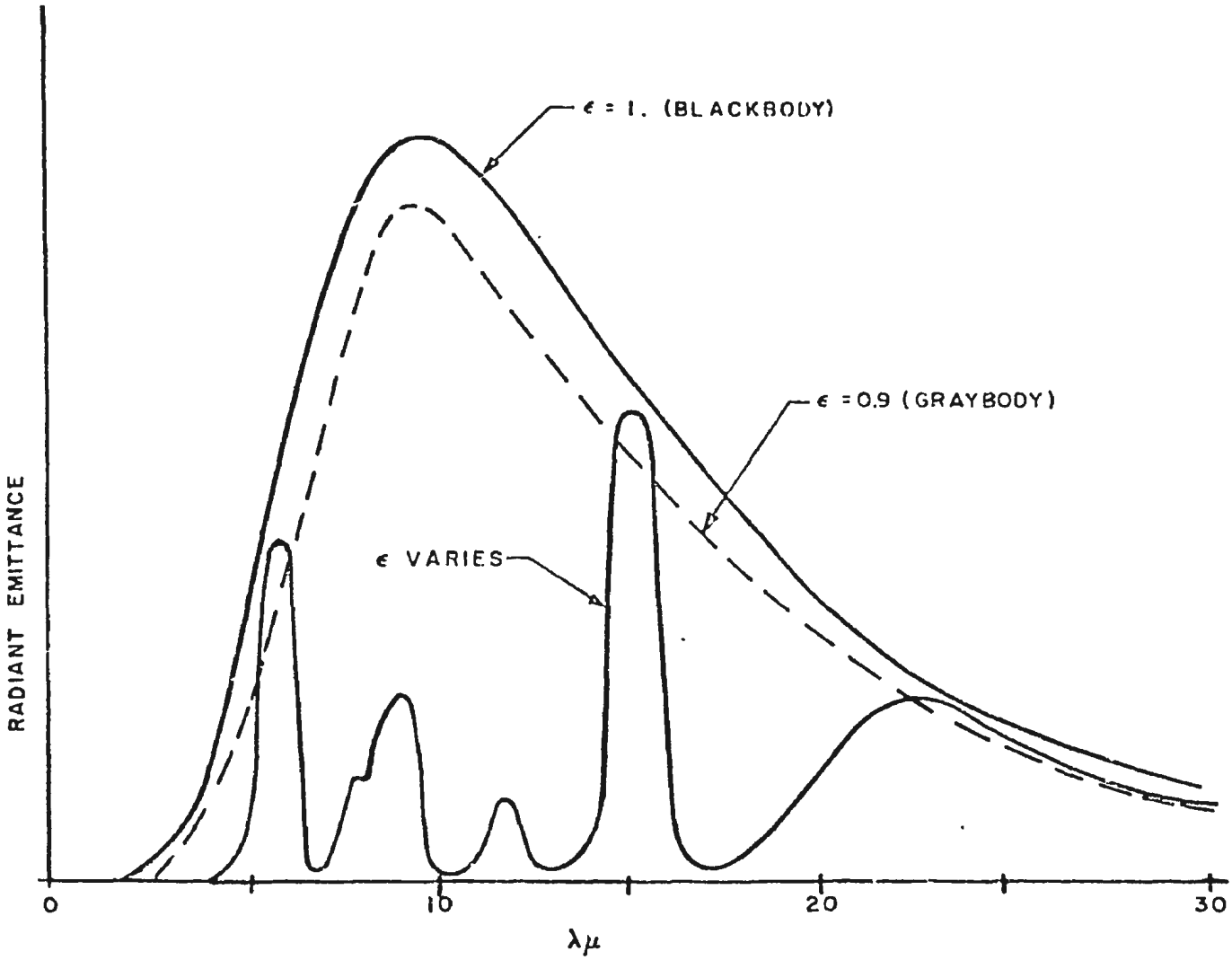

Figure 5 Spectral distribution curves illustrate characteristics of radiation from a blackbody with 1.0 emissivity, a graybody with 0.9 emissivity, and a body with an emissivity that varies with wavelength. (Barnes Engineering Company, 1970)

2.1.3.2 Total Power Law

When radiation is incident upon a body some of the radiation is transmitted, some absorbed and some reflected. The sum of the ratios of each of these terms must equal unity. This relationship is the power law and is stated as:

$$\alpha + \rho + \tau = 1 \qquad (9)$$

where, α = ratio of absorption to incident power

ρ = ratio of reflected to incident power

τ = ratio of transmitted to incident power

(Handbook of Military Infrared Technology, 1965)

which can also be written in terms of flux as:

$$\Phi_\alpha + \Phi_\rho + \Phi_\tau = \Phi \text{ incident} \qquad (10)$$

(Handbook of Military Infrared Technology, 1965)

For spectral quantities this relationship is written

$$\alpha(\lambda) + \rho(\lambda) + \tau(\lambda) = 1 \qquad (11)$$

(Handbook of Military Infrared Technology, 1965)

The conditions do not apply generally for two different components of polarization.

2.1.3.3 Kirchhoff's Law

This law was formulated from the comparison of absorbed and emitted radiation to that from perfect absorbers and perfect emitters. The law states that highly absorptive objects are also good radiators and complete absorbers are "perfect" radiators. For imperfect absorbers and radiators the ratio of energy absorbed by an object to the energy absorbed by a perfect absorber at the same temperature is the same as the ratio of energy emitted by that object to the energy emitted by a perfect radiator at the same temperature.

Historically, Kirchhoff's conclusions led to the concept of a "blackbody". Since no perfectly black material has ever been discovered a description of the radiation from physical objects must include a factor which is related to their degree of blackness. This factor is emissivity:

For two bodies in thermal equilibrium:

$$\alpha = \int_0^\infty \alpha(\lambda)\, d\lambda = \int_0^\infty \epsilon(\lambda)\, d\lambda = \epsilon \qquad (12)$$

$$\alpha(\lambda) = \epsilon(\lambda) \qquad (13)$$

$$\int_{\Delta\lambda} (\lambda)\, d\lambda = \int_{\Delta\lambda} (\lambda)\, d\lambda \qquad (14)$$

where ϵ = emissivity

α = absorptivity

(Handbook of Military Infrared Technology, 1965)

Equations 13 and 14 hold when the temperature on both sides of the equality is the same and the spectral region of consideration is the same for both α and ϵ. These relationships depend on the total power law and thermal equilibrium.

2.2 Natural Radiation and Backgrounds

The radiation from a target plus the radiation which is emitted by the sun, sky, cloud and terrain or ocean background comprises the total radiation received from a scene. This background radiation is called natural radiation. It can interfere with the recording of target radiation or temperatures.

2.2.1 Radiation of the Sky

The radiation of the sky as seen from the earth consists of several components. These are the sky spectral radiance, the overcast sky luminance, the ground level thermal irradiance of the sky, aurora and night airglow. Each could in part contribute to the background radiation on which an ice hazard target would have to be viewed against.

2.2.1.1 Sky Spectral Radiance

Sky-background radiation in the infrared is caused by scattering of the sun's radiation and by emission from atmospheric constituents. Figure 6 shows the separation of the infrared region into solar scattering and thermal emission regions. It can be seen that solar scattering is basically dominant in the middle infrared with emission becoming increasingly important as wavelength increases. At the boundary of the middle and far infrared (Figure 2) both scattering and emission have about equal importance. In the far infrared, emission is dominant with scattering effects quickly falling off around 8 μm.

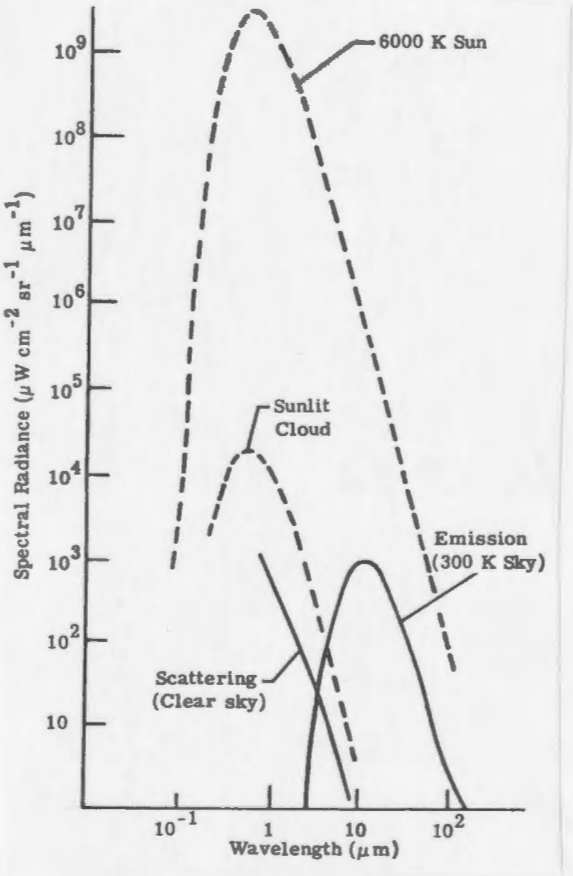

Figure 6 Contributions from scattering and atmospheric emission to background radiation. (Bell et al, 1960)

Figure 7 shows blackbody curves for various temperature ranges and equivalent spectral radiances. As the temperature increases at a particular wavelength the radiance increases. The simple model shows a peak in the vicinity of 10 μm which can also be seen in Figure 4 which is in agreement with the Planck Functions and Wien's Distribution Law.

Figure 8 shows the clear night radiance for different angles of elevation above the horizon. It can be seen that the radiation varies considerably from horizontal to vertical. In this data (Bell et al, 1960) it can be seen that at 6.3 μm and 15 μm the emission does not decrease as fast as say at, 10 μm. This is due to the presence of strong absorption-emission bands in the atmosphere. The same type of measurements taken in a humid sea level location as opposed to the dry mountain conditions of Figure 8 can be seen in Figure 9. Increased humidity and air mass reduces the spectral radiance of the sky. In both figures an emission peak can be seen at 9.6 μm. This is weaker than the peaks at 6.3 and 15 μm but it has an effect. In both figures emission shows a systematic decrease with increasing elevation.

Figure 10 shows the effect of the sun on both scattered and emissive radiation. As the elevation of

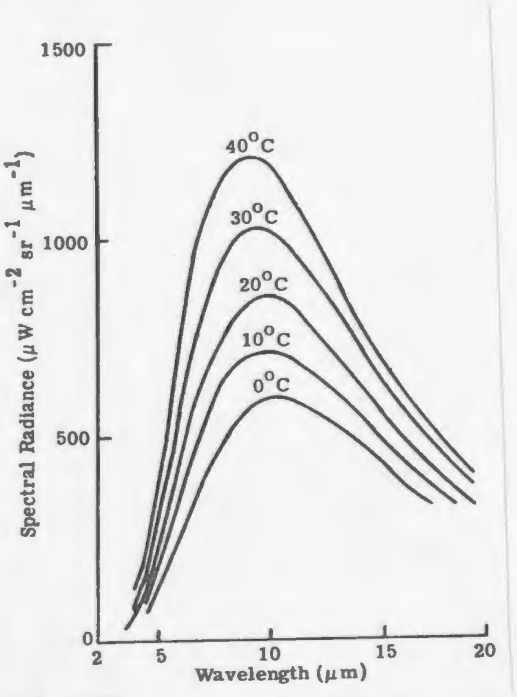

Figure 7 Spectral radiance of a blackbody with a temperature range of 0 to 40°C. (Bell et al, 1960)

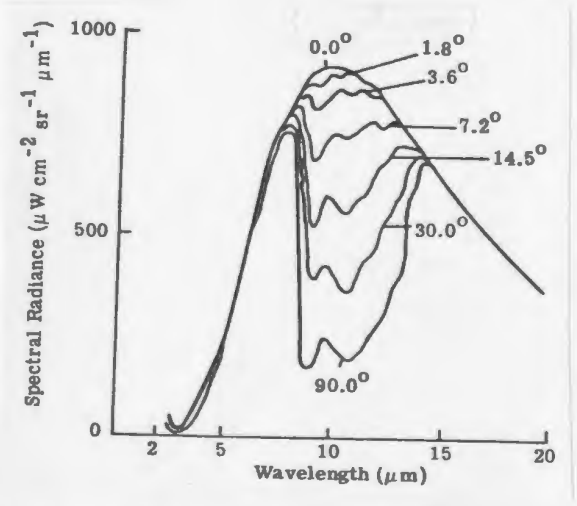

Figure 8 The spectral radiance of a clear nighttime sky. It is for several angles of elevation above the horizon. (Elk Park Station, Colorado) (Bell et al, 1960)

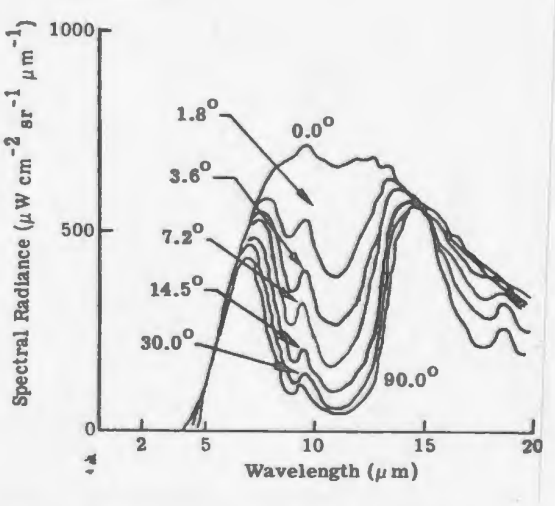

Figure 9 The spectral radiance of a clear nighttime sky. It is for several angles of elevation above the horizon. (Cocoa Beach, Florida) (Bell et al, 1960)

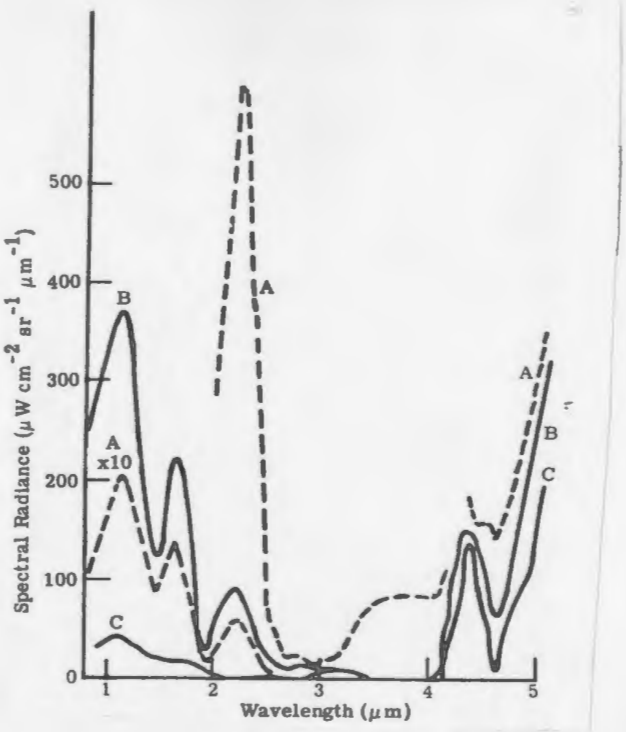

Figure 10 The spectral radiance of a clear zenith sky as a function of the sun position. Curve A = sun elevation 77°, temperature 30°C; curve B = sun elevation 41°, temperature 25.5°C; curve C = sun elevation 15°, temperature 26.5°C. (Bell et al, 1960)

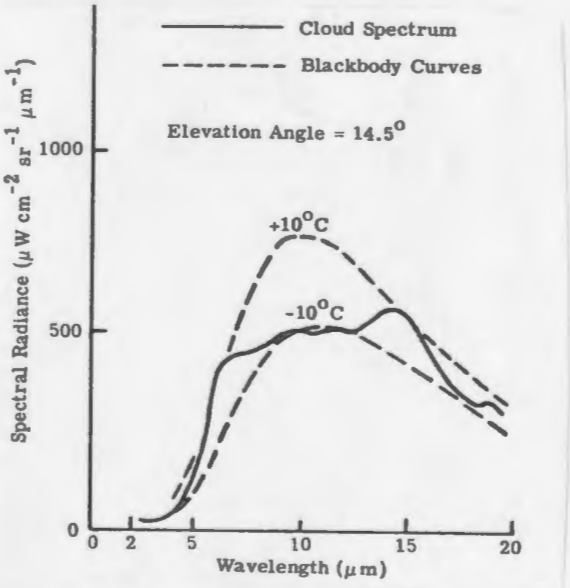

Figure 11 The spectral radiance of the underside of a dark cumulus cloud. (Bell et al, 1960)

the sun decreases the scattered radiation varies considerably while the emission in the thermal region, beginning at about 4 μm has little change.

The presence of clouds affects both the scatter and emission regions. In the scatter or solar region the position of the sun, observer and cloud cover are important because of strong forward scattering. As the sky becomes heavy and overcast multiple scattering reduces the forward scattering effect. Thick clouds are good blackbodies and in the 8 to 14 μm region they are good emitters. Absorption-emission bands at 6.3 and 15.0 μm can cause a cloud not to be visible to infrared instrumentation thus the radiation in these regions is determined by the temperature of the atmosphere. This can be seen in Figure 11. In this figure the temperature of the atmosphere is $+10^{o}$ C and the temperature of the underside of the cloud is -10^{o} C. Blackbody curves are drawn for both temperatures. The radiation from the cloud in the region 8 to 13 μm approaches the cloud blackbody temperature.

Figure 12 shows sky radiation variations as a function of elevation angle. Figure 13 shows radiance variations due to seasons.

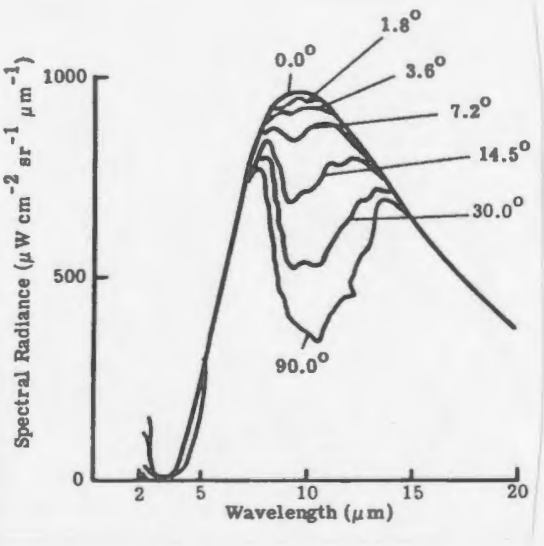

Figure 12 The spectral radiance of sky covered with cirrus clouds at several angles of elevation. (Bell et al, 1960)

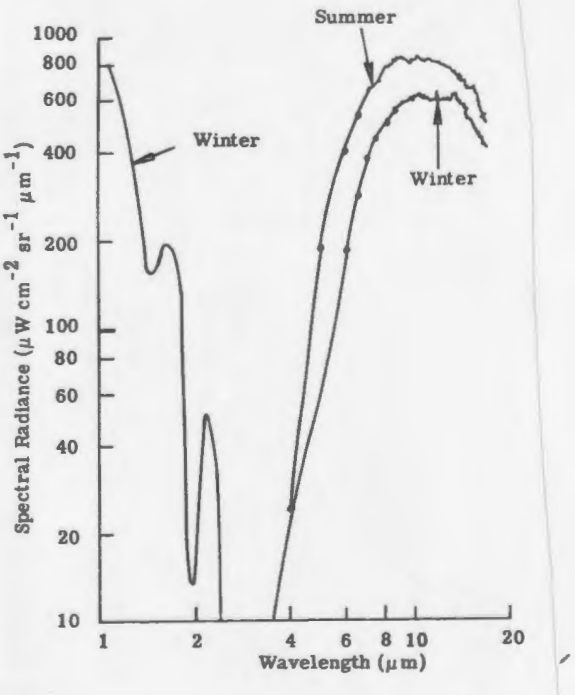

Figure 13 Spectral radiance of overcast skies in winter and summer. (Bell et al, 1956)

2.2.1.2 Overcast Sky Luminance

An approximate relation for the overcast sky luminance as viewed from ground level is given as:

$$L_v(\theta) = L_v(\text{horizon})\,(1 + A\cos\theta) \qquad (15)$$

where θ = angle from zenith

$A = 2.0$, but

$= 1.0$ for arctic skies and over snow (Gordon and Church, 1966)

(Infrared Handbook, 1978)

2.2.1.3 Ground Level Thermal Irradiance of the Sky

The total thermal irradiance of a clear sky at sea level, E(Sky), can be estimated using the empirical relation with the ground-level meteorological absolute air temperature, T_a:

$$E(\text{sky}) = \sigma T_a^4\,(1-0.261\exp(-7.77\times 10^{-4}(273-T_a)^2)) \qquad (16)$$

(Infrared Handbook, 1978)

The absorption bands on each side of the 8 to 14 μm atmospheric window will emit most of the irradiance (Idso and Jackson, 1969).

2.2.1.4 Aurora

Aurora emission lines occur at 0.92, 1.04 and 1.11 μm (Figure 14). The emission measurement of aurora and airglow is difficult beyond 2.0 μm because of absorption and thermal processes in the atmosphere. Figures 15 and 16 show high-altitude rocket borne spectrometer results for short wavelength infrared (SWIR) and long wavelength infrared (LWIR) of aurora spectral radiance.

Figure 17 shows the geographic distribution of frequency of aurora in the northern hemisphere. The isochasms refer to the number of nights during the year in which an aurora might be seen at some time during the night in any part of the sky if clouds and other factors affecting visual detection do not interfere.

2.2.1.5 Night Airglow

Airglow is defined as the nonthermal radiation emitted by the earth's atmosphere. Exceptions are auroral emissions and cataclysmic radiation due to lightning, meteor trails etc. Night airglow emissions in the infrared are caused by transitions between vibrational states of the OH^- radical. The exact

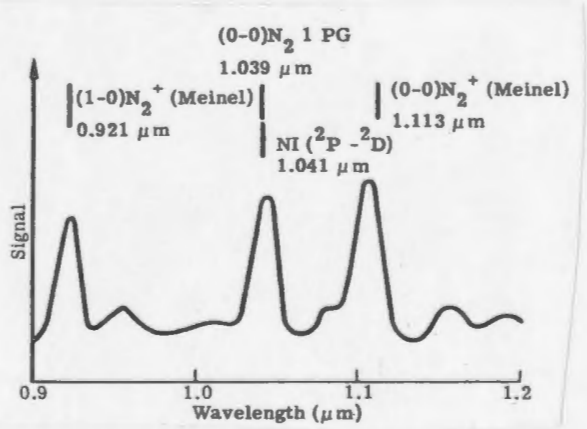

Figure 14 Auroral spectrum, 0.9 to 1.2 μm. It was obtained with a lead sulfide spectrometer; projected silt width 100 Å. (Harrison and Jones, 1977)

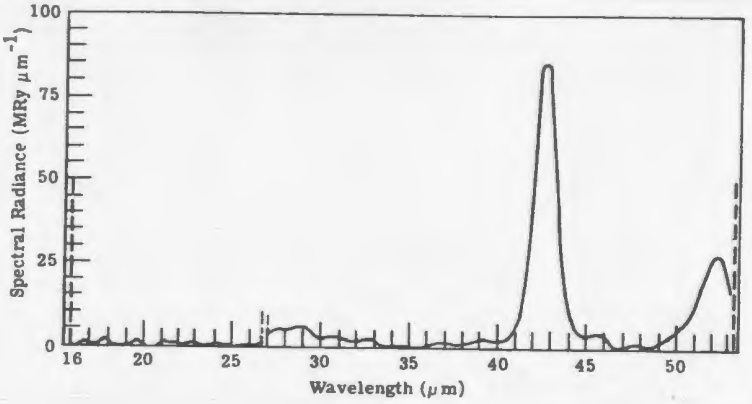

(a) Paiute Tomahawk 10.205-2 97km.

NOTE: The unit MRy is a megarayleigh (see list of symbols)

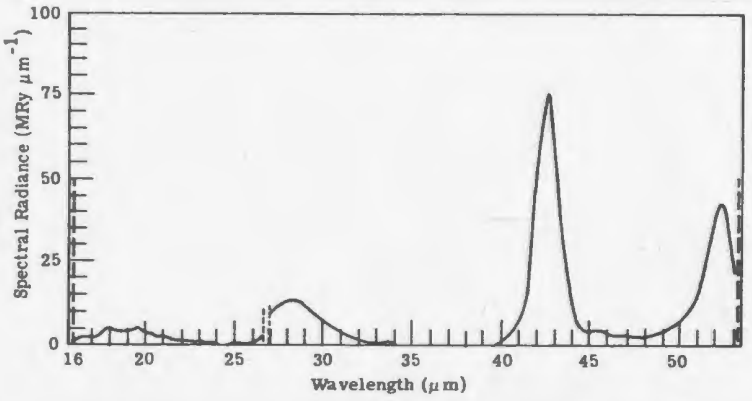

(b) Paiute Tomahawk 10.205-2 86km x 10^{-1}

Figure 15 Sample spectra scans from a SWIR spectometer aboard a Paiute-Tomahawk rocket launched from Poker Flat, Alaska, 24 March 73. Although uncorrected for actual rocket aspect, the data approximate the zenith radiance. (Stairs et al, 1975)

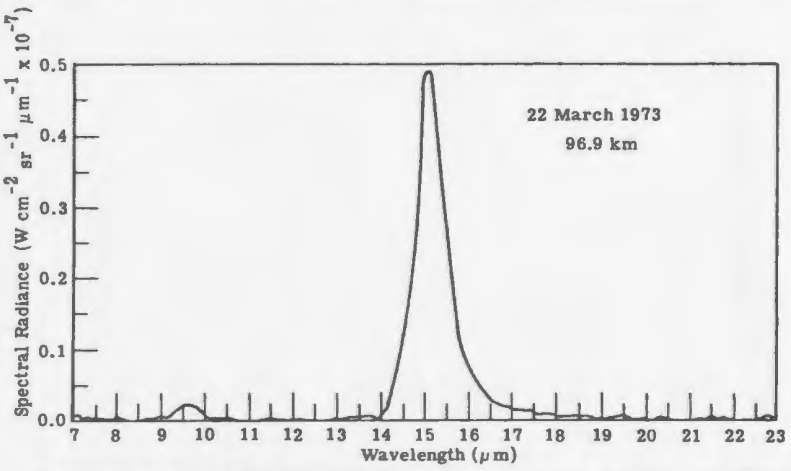

Figure 16 Sample spectrum scan (vertical from a LWIR spectrometer aboard a Black Brant rocket flown from Poker Flat, Alaska, 22 March 73. The rocket altitude is 96.9 km on rocket descent. (Stairs et al, 1975)

Figure 17 Geographic distribution of the frequency of aurora in the northern hemisphere. (Vestine, 1944)

mechanism of excitation is still unclear but the effect is to release energy from solar radiation stored during the daytime. Airglow occurs at all latitudes.

There is evidence that airglow is related to the distribution of ozone. Measured heights of airglow range from 70.0 to 90.0 km which corresponds to the location of ozone.

Nightglow increases away from zenith at approximately sec θ. Measurements are usually normalized to zenith. As airglow is defined as nonthermal emissions it is reported in the 1.0 to 4.0 μm solar scattering region.

2.2.2 Marine Backgrounds

The radiance of the sea surface is the sum of its thermal emission and reflected incident radiation. The factors that determine the character of the marine background are:

1) Optical properties of water,
2) Surface geometry and wave-slope distribution,
3) Surface temperature distribution, and
4) Properties of bottom material.

Atmospheric scattering, transmission and emission from scene to observing instrument contribute significantly to observed radiances.

2.2.2.1 Optical Properties of Water in the Thermal Range

Essentially, water is opaque to infrared radiation at wavelengths longer than 3 μm. The absorption coefficient is of such a magnitude that the surface layer, 0.01 cm thick, determines the thermal radiance of the water. Subsurface scattering of sky radiation is absent in the thermal range. There is no significant difference in the transmittance of sea and distilled water in the thin surface layer in the 2 to 15 μm region. Figure 18 shows the transmittance curve, Figure 19 the index of refraction for water, Figure 20 and 21 reflection and emissivity data and Figures 22 and 23 absorption data for sea water.

2.2.2.2 Sea Surface Geometry

Figure 24 shows the effect of wave slope on the reflectance of a sea surface roughened by a Beaufort 4 wind (11 to 16 Kt, white caps). Reflectance approaches 20% near the horizon thus emissivity remains at 80% or higher. Figure 25 gives the radiance of the sea surface

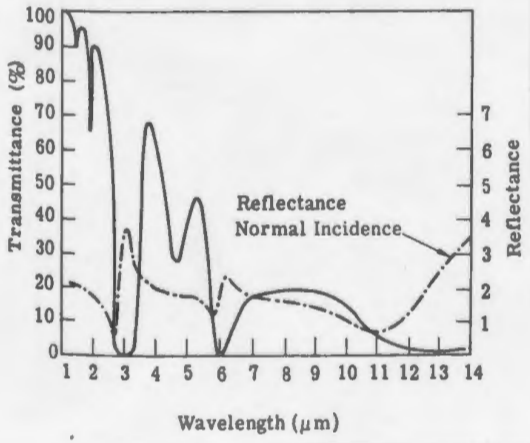

Figure 18 Transmittance of 0.002 cm of sea water and reflectance of of a free sea-water surface. (The Infrared Handbook, 1978)

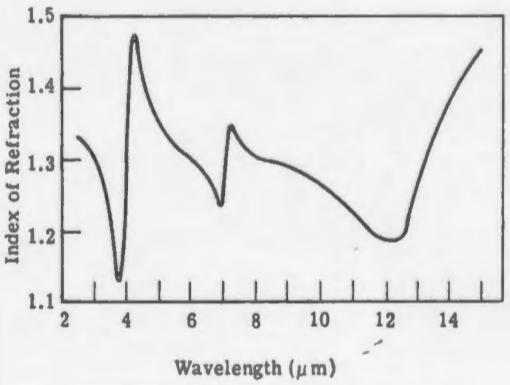

Figure 19 Indices of refraction of water calculated from reflectivity data. (The Infrared Handbook 1978)

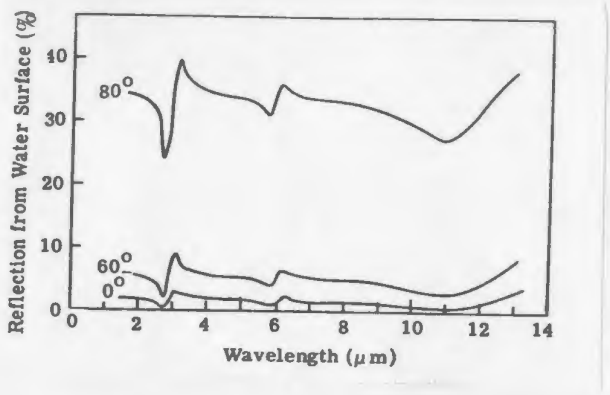

Figure 20 Reflection from a water surface at 10^{0}, 60^{0} and 80^{0} angle of incidence calculated. (The Infrared handbook, 1978)

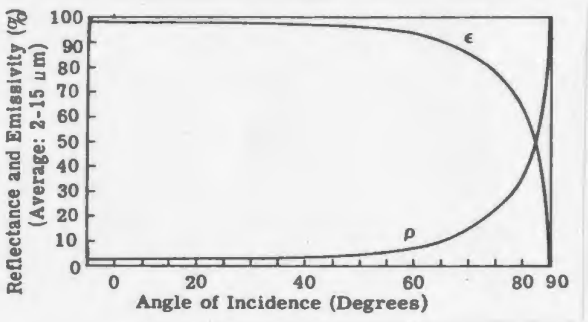

Figure 21 Reflectance and emissivity of water (2 to 15 μm average) versus angle of incidence, calculated from average data. (Note the scale change) (McMahon, 1950)

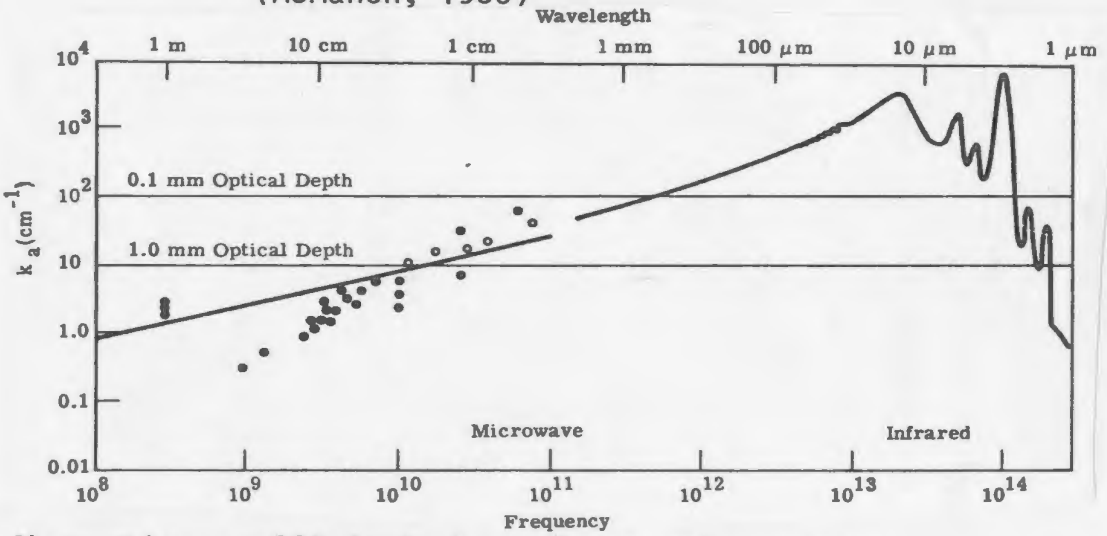

Figure 22 Absorption coefficient, k_a, of sea water versus wavelength. (Ewing, 1965)

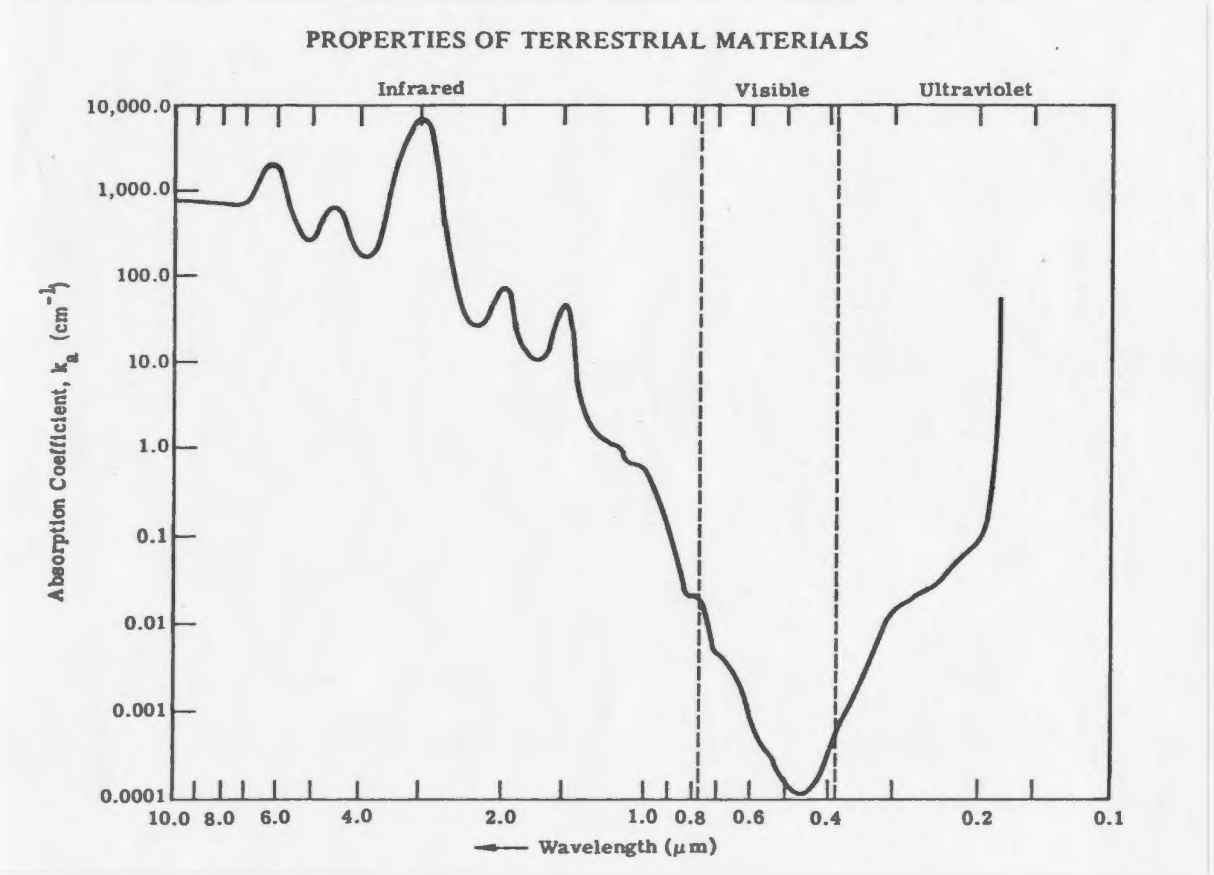

Figure 23 Absorption of radiation by sea water, (Ewing, 1965)

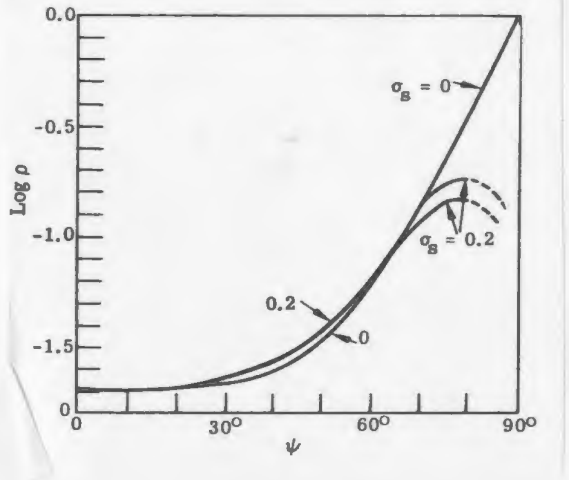

Figure 24 Reflection of solar radiation from a flat surface ($\sigma_s = 0$) and a surface roughened by a beaufort 4 wind ($\sigma_s = 0.2$). The albedo, ρ, varies from 0.2 for a zenith sun, (ψ=0°) to unity for the sun at the horizon (ψ= 90°) on a flat sea surface. For a rought surface, shadowing and multiple reflections become important factors when the sun is low. The lower and upper branches of the curve marked $\sigma_s = 0.2$ represent two assumptions regarding the effect of multiple reflection. True values are expected to lie between the indicated limits. (Cox and Munk, 1956)

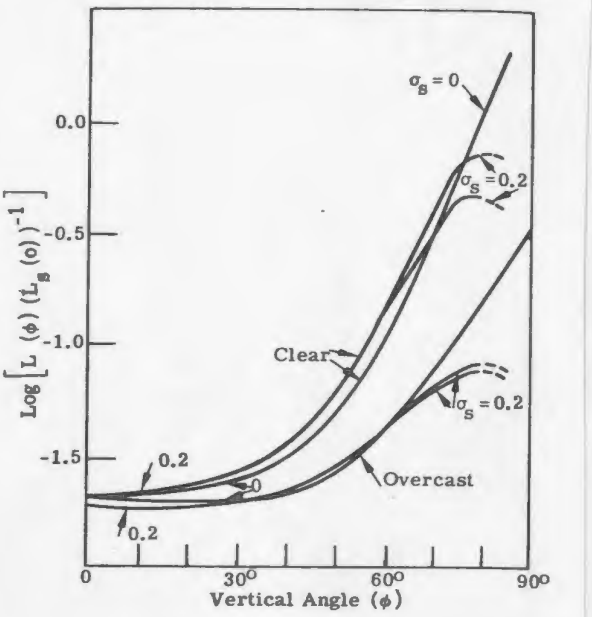

Figure 25 The radiance of the sea surface, L(Ø), divided by sky radiance at the zenith, L_s(Ø), as a function of the angle Ø. The curves are computed for a flat (σ_s=0) and rough (σ_s=0.2) surface for two of the sky conditions. (Cox and Munk, 1956)

along an azimuth 90^{o} from that of the sun. There is a lack of similar observations for the radiance of the sea surface at night. The variation of the sky radiance with zenith angle is similar for day and night and photographic reflectance is about equal to the average for the infrared from 2 to 15 μm (Figure 20). Therefore, Figure 25 shows the general shape of that part of the radiance of the sea surface at night caused by the reflection of sky radiation. The addition of the sea surface infrared radiance due to thermal emission must be added to these curves. Figures 26, 27 and 28 are examples of sea spectral radiance.

2.2.2.3 Sea Surface Temperature Distribution

The temperature of the sea surface determines the contribution of emission to its total radiance. Currents will produce anomalies of several degrees as they intermix with other currents (Ketchen, LaViolette and Worsfold, 1977). In most infrared scenes of marine interest the radiance variation from point to point is the value that determines the background against which a target is seen. Reflected sky radiance can sometimes predominate. Figure 29 shows a typical surface temperature profile for the sea for the first 50 millimeters.

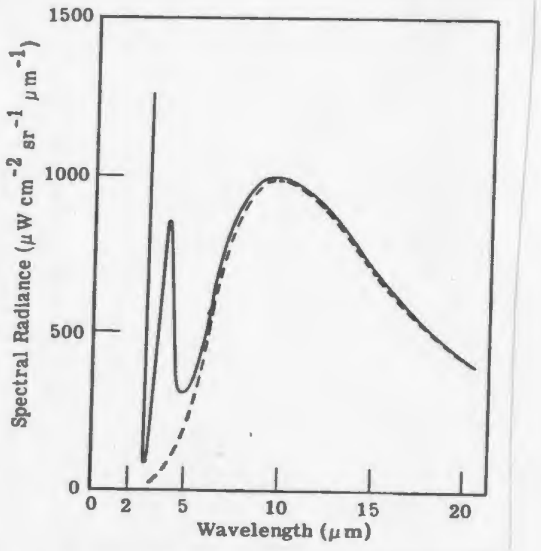

Figure 26 Spectral radiance of the Banana River at Cocoa Beach, Florida (Bell et al, 1962)

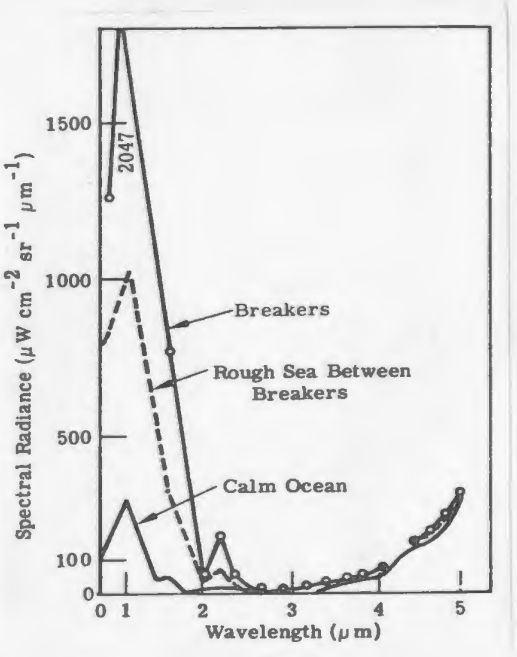

Figure 27 Spectral radiance of the Ocean. (Bell et al, 1962)

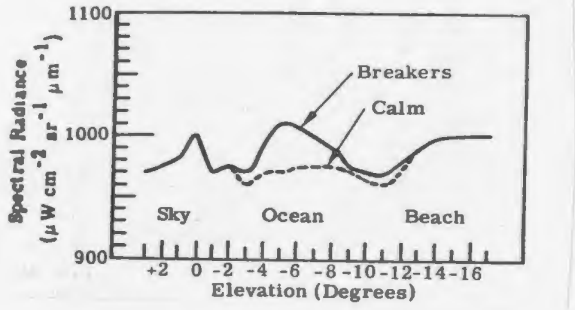

Figure 28 Spectral radiance of the ocean versus the elevation angle. (Bell et al, 1962)

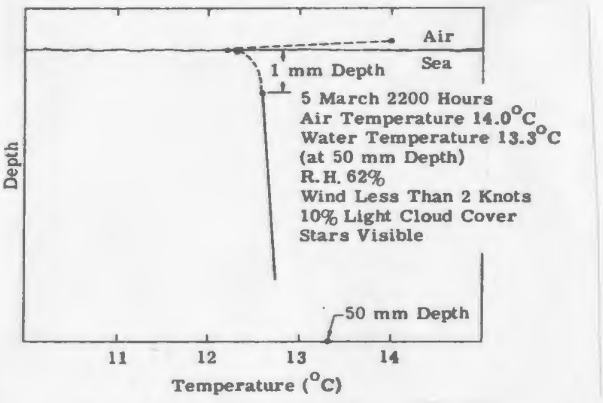

Figure 29 Thermal structure of the sea boundary layer. Previous conditions: 12h cool (12 to 15°C), no rain. The data were taken during the passage of a warm front. (Ewing and McAlister, 1960)

2.2.3 Snow

Snow is a common surface cover at high latitudes. It differs from place to place and from time to time by differences in the crystal sizes, the state of division of flakes, the compactness or density of snow cover, and the amount of free water within the snow cover. New-fallen snow can be considered to reflect or emit radiation diffusely but old snow may develop a roughened compacted crust which results in less diffuse or specular radiation. Data may be found in O'Brien et al (1975). All work has been done in the near infrared. No data is available for the 8-14 μm region.

2.2.4 Sun

The values in Table 1 give standard solar spectral irradiance at the earth's mean distance from the sun. Figure 30 shows the spectral irradiance of exoatmospheric solar radiation. The spectral irradiance at sea level for solar atmospheric air masses are given in Table 2. Figures 31 and 32 show variation of spectral radiance due to various air masses and Figure 33 shows global and direct solar spectral irradiance on a horizontal surface for various slant paths.

Table 1 Solar Spectral Irradiance - Proposed Standard Curve. (Thekakara, 1972)

λ	- Wavelength in micrometers
E_λ (λ)	- Solar spectral irradiance averaged over small bandwidth centered at λ, in W m^{-2} μm^{-1}
$D(0-\lambda)$	- Percentage of the solar constant associated with wavelengths shorter than λ
Solar Constant	- 1353 W m^{-2}

λ	E_λ (λ)	$D(0-\lambda)$	λ	E_λ (λ)	$D(0-\lambda)$	λ	E_λ (λ)	$D(0-\lambda)$
0.120	0.100	0.00044	0.375	1157.0	6.582	0.575	1719.0	32.541
0.140	0.030	0.00053	0.380	1120.0	7.003	0.580	1715.0	33.176
0.150	0.07	0.00057	0.385	1098.0	7.413	0.585	1712.0	33.809
0.160	0.23	0.00068	0.390	1098.0	7.819	0.590	1700.0	34.439
0.170	0.63	0.00100	0.395	1189.0	8.241	0.595	1682.0	35.064
0.180	1.25	0.00169	0.400	1429.0	8.725	0.600	1666.0	35.683
0.190	2.71	0.00316	0.405	1644.0	9.293	0.605	1647.0	36.295
0.200	10.7	0.00811	0.410	1751.0	9.920	0.610	1635.0	36.902
0.210	22.9	0.02053	0.415	1774.0	10.571	0.620	1602.0	38.098
0.220	57.5	0.05024	0.420	1747.0	11.222	0.630	1570.0	39.270
0.225	64.9	0.0728	0.425	1693.0	11.858	0.640	1544.0	40.421
0.230	66.7	0.0971	0.430	1639.0	12.473	0.650	1511.0	41.550
0.235	59.3	0.1204	0.435	1663.0	13.083	0.660	1486.0	42.657
0.240	63.0	0.1430	0.440	1810.0	13.725	0.670	1456.0	43.744
0.245	72.3	0.1680	0.445	1922.0	14.415	0.680	1427.0	44.810
0.250	70.4	0.1944	0.450	2006 0	15.140	0.690	1402.0	45.855
0.255	104.0	0.2266	0.455	2057.0	15.891	0.700	1369.0	46.879
0.260	130.0	0.2698	0.460	2066.0	16.653	0.710	1344.0	47.882
0.265	185.0	0.3280	0.465	2048.0	17.413	0.720	1314.0	48.864
0.270	232.0	0.4051	0.470	2033.0	18.167	0.730	1290.0	49.826
0.275	204.0	0.4857	0.475	2044.0	18.921	0.740	1260.0	50.769
0.280	222.0	0.5644	0.480	2074.0	19.681	0.750	1235.0	51.691
0.285	315.0	0.6636	0.485	1976.0	20.430	0.760	1211.0	52.595
0.290	482.0	0.8109	0.490	1950.0	31.155	0.770	1185.0	53.480
0.295	584.0	1.0078	0.495	1960.0	21.878	0.780	1159.0	54.346
0.300	514.0	1.2107	0.500	1942.0	22.599	0.790	1134.0	55.194
0.305	603.0	1.4171	0.505	1920.0	23.312	0.800	1109.0	56.023
0.310	689.0	1.6558	0.510	1882.0	24.015	0.810	1085.0	56.834
0.315	764.0	1.9243	0.515	1833.0	24.701	0.820	1060.0	57.627
0.320	830.0	2.2188	0.520	1833.0	25.379	0.830	1036.0	58.401
0.325	975.0	2.552	0.525	1852.0	26.059	0.840	1013.0	59.158
0.330	1059.0	2.928	0.530	1842.0	26.742	0.850	990.0	59.899
0.335	1081.0	3.323	0.535	1818.0	27.418	0.860	968.0	60.622
0.340	1074.0	3.721	0.540	1783.0	28.084	0.870	947.0	61.330
0.345	1069.0	4.117	0.545	1754.0	28.737	0.880	926.0	62.022
0.350	1093.0	4.517	0.550	1725.0	29.380	0.890	908.0	62.700
0.355	1083.0	4.919	0.555	1720.0	30.017	0.900	891.0	63.365
0.360	1068.0	5.316	0.560	1695.0	30.648	0.910	880.0	64.019
0.365	1132.0	5.723	0.565	1705.0	31.276	0.920	869.0	64.665
0.370	1181.0	6.150	0.570	1712.0	31.907	0.930	858.0	65.304

Table 1 Solar Spectral Irradiance - Proposed Standard Curve. (Thekakara, 1972) (Continued)

λ - Wavelength in micrometers
$E_\lambda(\lambda)$ - Solar spectral irradiance averaged over small bandwidth centered at λ, W m^{-1} μm^{-1}
$D(0-\lambda)$ - Percentage of the solar constant associated with wavelengths shorter than λ
Solar Constant - 1353 W m^{-2}

λ	$E_\lambda(\lambda)$	$D(0-\lambda)$	λ	$E_\lambda(\lambda)$	$D(0-\lambda)$	λ	$E_\lambda(\lambda)$	$D(0-\lambda)$
0.940	847.0	65.934	2.40	62.0	95.8580	9.0	0.380	99.913939
0.950	837.0	66.556	2.50	55.0	96.2903	10.0	0.250	99.937221
0.960	820.0	67.168	2.60	48.0	96.6710	11.0	0.170	99.952742
0.970	803.0	67.768	2.70	43.0	97.0073	12.0	0.120	99.963459
0.980	785.0	68.355	2.80	39.0	97.3103	13.0	0.087	99.971108
0.990	767.0	68.928	2.90	35.0	97.5838	14.0	0.055	99.976356
1.000	748.0	69.488	3.00	31.0	97.8277	15.0	0.049	99.980199
1.050	668.0	72.105	3.10	26.0	98.0383	16.0	0.038	99.983414
1.100	593.0	74.435	3.20	22.6	98.2179	17.0	0.031	99.985964
1.150	535.0	76.519	3.30	19.2	98.3724	18.0	0.024	99.987997
1.200	485.0	78.404	3.40	16.6	98.5047	19.0	0.02000	99.989623
1.250	438.0	80.109	3.50	14.6	98.6200	20.0	0.01600	99.990953
1.300	397.0	81.652	3.60	13.5	98.7238	25.0	0.00610	99.995037
1.350	358.0	83.047	3.70	12.3	98.8192	30.0	0.00300	99.996718
1.400	337.0	84.331	3.80	11.1	98.9056	35.0	0.00160	99.997568
1.450	312.0	85.530	3.90	10.3	98.9847	40.0	0.00094	99.998037
1.500	288.0	86.639	4.00	9.5	99.0579	50.0	0.00038	99.998525
1.550	267.0	87.665	4.10	8.7	99.1252	60.0	0.00019	99.998736
1.600	245.0	88.611	4.20	7.8	99.1861	80.0	0.00007	99.998928
1.650	223.0	89.475	4.30	7.1	99.2412	100.0	0.00003	99.999002
1.70	202.0	90.261	4.40	6.5	99.291507	1000.0	0.00000	100.000000
1.75	180.0	90.967	4.50	5.9	99.337331	--	-	-
1.80	159.0	91.593	4.60	5.3	99.378721	-	-	-
1.85	142.0	92.149	4.70	4.8	99.416045	-	-	-
1.90	126.0	92.644	4.80	4.5	99.450413	-	-	-
1.95	114.0	93.088	4.90	4.1	99.482195	-	-	-
2.00	103.0	93.489	5.00	3.83	99.511500	-	-	-
2.10	90.0	94.202	6.00	1.75	99.717708	-	-	-
2.20	79.0	94.826	7.00	0.99	99.818965	-	-	-
2.30	69.0	95.373	8.00	0.60	99.877723	-	-	-

Table 2 Solar Irradiance at Sea Level on an Area Normal to the Sun for m = 2, E_0 = 1322W m^{-2} (Moon, 1940)

λ (μm)	$E_\lambda(\lambda)$ (W $m^{-2}\mu m^{-1}$)	λ (μm)	$E_\lambda(\lambda)$ (W $m^{-2}\mu m^{-1}$)	λ (μm)	$E_\lambda(\lambda)$ (W $m^{-2}\mu m^{-1}$)	λ (μm)	$E_\lambda(\lambda)$ (W $m^{-2}\mu m^{-1}$)
0.301	0.177	0.510	1206.0	0.91	375.0	1.31	203.0
0.302	0.342	0.520	1199.0	0.92	258.0	1.32	168.0
0.303	0.647	0.530	1188.0	0.93	169.0	1.33	115.0
0.304	1.16	0.540	1198.0	0.94	278.0	1.34	58.1
0.305	1.91	0.550	1190.0	0.95	487.0	1.35	18.1
0.306	2.89	0.560	1182.0	0.96	584.0	1.36	0.660
0.307	4.15	0.570	1178.0	0.97	633.0	1.37	–
0.308	6.11	0.580	1168.0	0.98	645.0	1.38	–
0.309	8.38	0.590	1161.0	0.99	643.0	1.39	–
0.310	11.0	0.600	1167.0	1.00	630.0	1.40	–
0.311	13.9	0.61	1168.0	1.01	620.0	1.41	1.91
0.312	17.2	0.62	1165.0	1.02	610.0	1.42	3.72
0.313	21.0	0.63	1176.0	1.03	601.0	1.43	7.53
0.314	25.4	0.64	1175.0	1.04	592.0	1.44	13.7
0.315	30.0	0.65	1173.0	1.05	551.0	1.45	23.8
0.316	34.8	0.66	1166.0	1.06	526.0	1.46	30.5
0.317	39.8	0.67	1160.0	1.07	519.0	1.47	45.1
0.318	44.9	0.68	1149.0	1.08	512.0	1.48	83.7
0.319	49.5	0.69	978.0	1.09	514.0	1.49	128.0
0.320	54.0	0.70	1108.0	1.10	252.0	1.50	157.0
–	–	0.71	1070.0	1.11	126.0	1.51	187.0
–	–	0.72	832.0	1.12	69.9	1.52	209.0
0.330	101.0	0.73	965.0	1.13	98.3	1.53	217.0
0.340	151.0	0.74	1041.0	1.14	164.0	1.54	226.0
0.350	188.0	0.75	867.0	1.15	216.0	1.55	221.0
0.360	238.0	0.76	566.0	1.16	271.0	1.56	217.0
0.370	279.0	0.77	968.0	1.17	328.0	1.57	213.0
0.380	336.0	0.78	907.0	1.18	346.0	1.58	209.0
0.390	397.0	0.79	923.0	1.19	344.0	1.59	205.0
0.400	470.0	0.80	857.0	1.20	373.0	1.60	202.0
0.410	672.0	0.81	698.0	1.21	402.0	1.61	198.0
0.420	733.0	0.82	801.0	1.22	431.0	1.62	194.0
0.430	787.0	0.83	863.0	1.23	420.0	1.63	189.0
0.440	911.0	0.84	858.0	1.24	387.0	1.64	184.0
0.450	1006.0	0.85	839.0	1.25	328.0	1.65	173.0
0.460	1080.0	0.86	813.0	1.26	311.0	1.66	163.0
0.470	1138.0	0.87	798.0	1.27	331.0	1.67	159.0
0.480	1183.0	0.88	614.0	1.28	382.0	1.68	145.0
0.490	1210.0	0.89	517.0	1.29	346.0	1.69	139.0
0.500	1215.0	0.90	480.0	1.30	264.0	1.70	132.0

Table 2 Solar Irradiance at Sea Level on an Area Normal to the Sun for m = 2, E_0 = 1322W m^{-2} (Moon, 1940) (Continued)

λ (μm)	$E_\lambda(\lambda)$ (W $m^{-2}\mu m^{-1}$)	λ (μm)	$E_\lambda(\lambda)$ (W $m^{-2}\mu m^{-1}$)	λ (μm)	$E_\lambda(\lambda)$ (W $m^{-2}\mu m^{-1}$)	λ (μm)	$E_\lambda(\lambda)$ (W $m^{-2}\mu m^{-1}$)
1.71	124.0	1.82	–	1.93	3.68	2.04	54.70
1.72	115.0	1.83	–	1.94	5.30	2.05	38.3
1.73	105.0	1.84	–	1.95	17.7	2.06	56.2
1.74	97.1	1.85	–	1.96	31.7	2.07	77.0
1.75	80.2	1.86	–	1.97	37.7	2.08	88.0
1.76	58.9	1.87	–	1.98	22.6	2.09	86.8
1.77	38.8	1.88	–	1.99	1.58	2.10	85.6
1.78	18.4	1.89	–	2.00	2.66	2.11	84.4
1.79	5.70	1.90	–	2.01	19.50	2.12	83.2
1.80	0.920	1.91	0.705	2.02	47.60	2.13	20.7
1.81	–	1.92	2.34	2.03	55.40	2.14	–

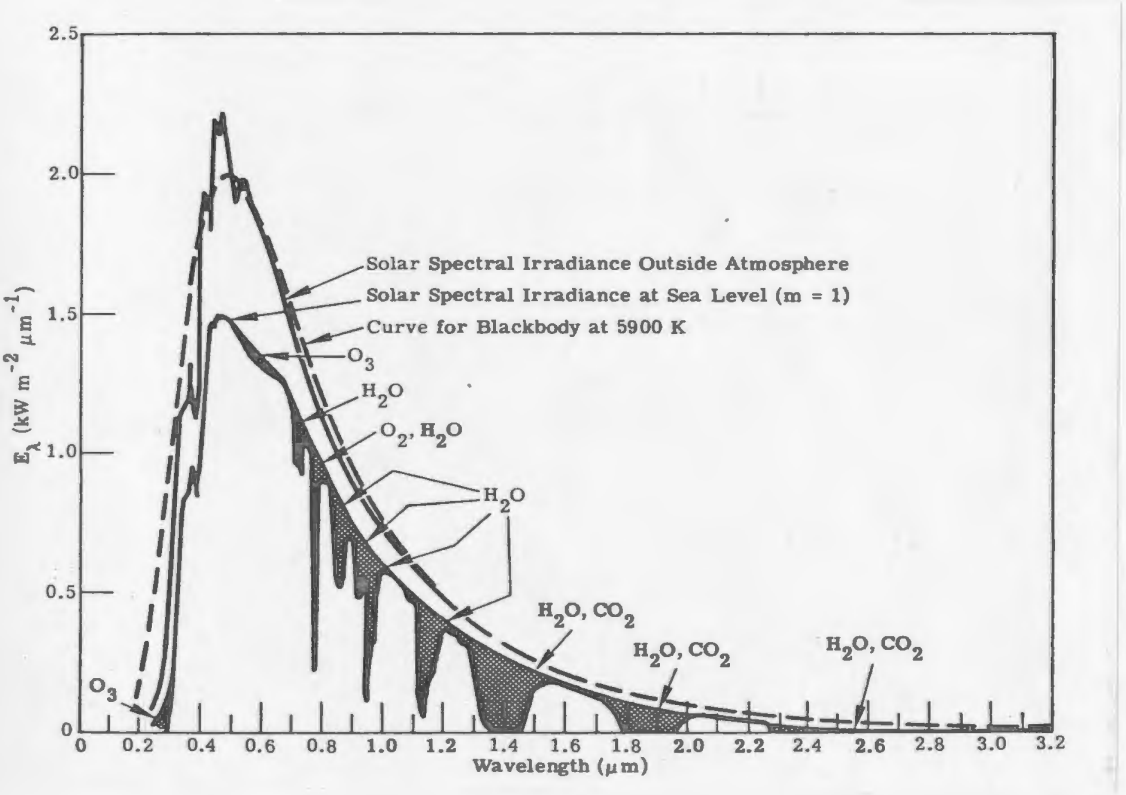

Figure 30 Spectral distribution curves related to the sun. The shaded areas indicate absorption at sea level due to the atmospheric constituents shown. (The Infrared Handbook, 1978)

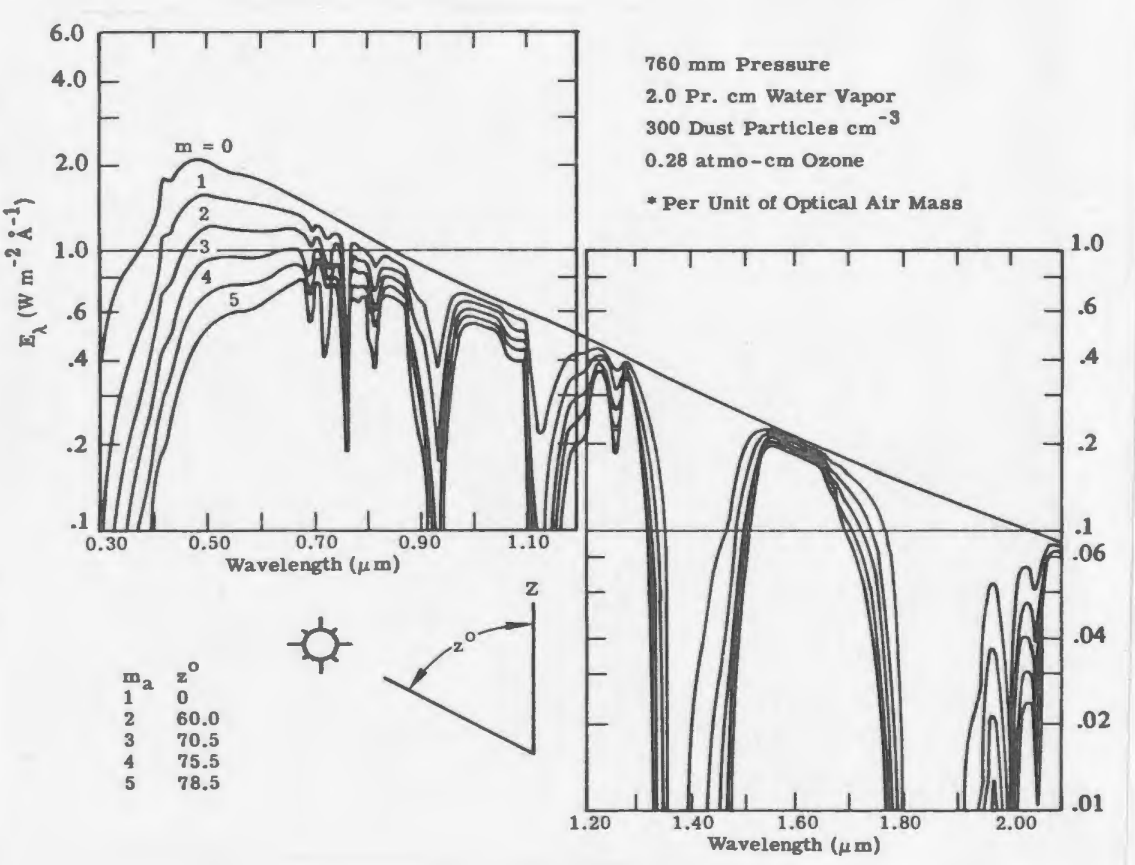

Figure 31 Solar spectral irradiance curves at sea level for various optical air masses. The value of the solar constant used in this calculation was 1322W m^{-2} (Moon, 1940)

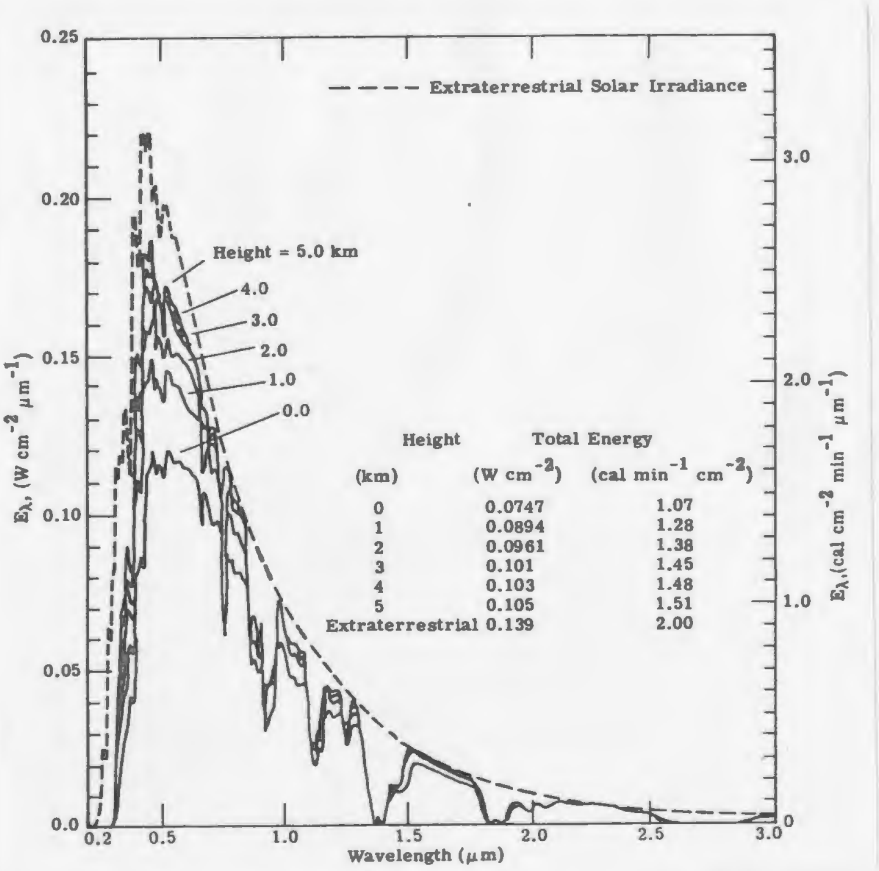

Figure 32 Variation with altitude of spectral intensity versus wavelength for direct solar radiation perpendicular to the sun's rays for an air mass of 1.5. (Gates, 1966)

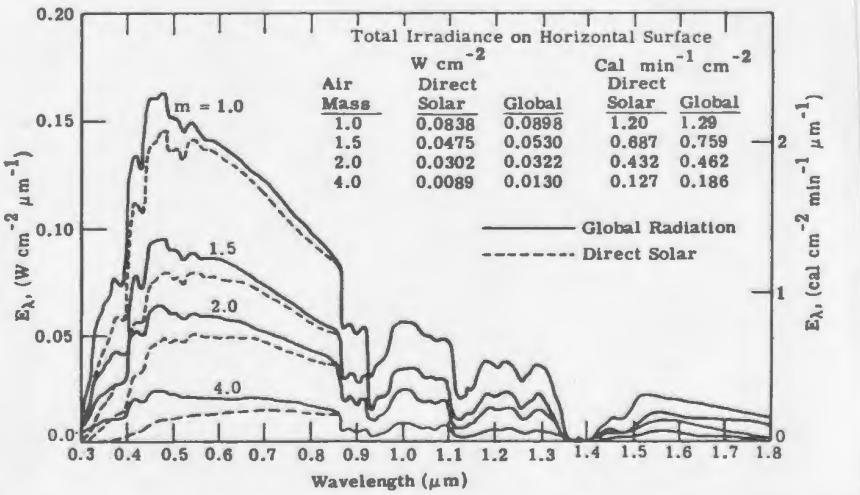

Figure 33 Spectral distribution as a function of wavelength of the global and direct solar radiation incident at sea level on a horizontal surface for various slant paths corresponding to air mass 1.0, 1.5, 2.0 and 4.0. (Gates, 1966)

2.2.5 The Earth As Seen From Space

Emission from the earth depends upon the diurnal variations of the sun's irradiance. An object viewed during the day emits more irradiance than an object viewed at night. This is due to the solar heating and thermal inertia effects. A target viewed at night after the solar effects have been emitted represents the passive radiance of the target alone. Diurnal variations can be seen in Figure 34 for various materials.

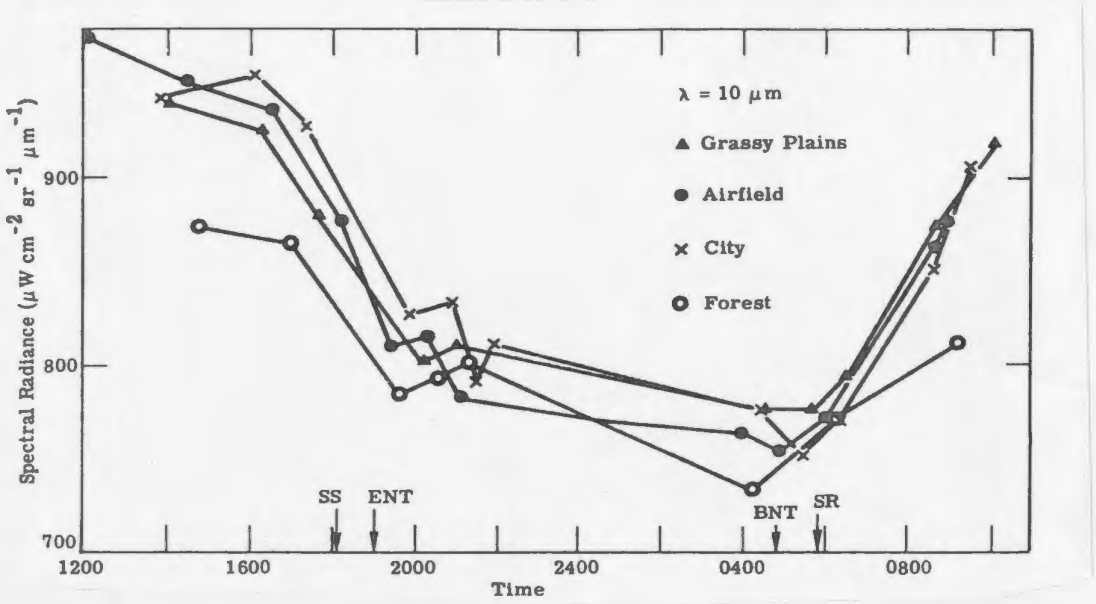

Figure 34 Diurnal variation in the 10 μm Radiance of selected backgrounds. SS = sunset; SR = sunrise; ENT = end of nautical twilight; BNT = beginning of nautical twilight. (Bell et al, 1962)

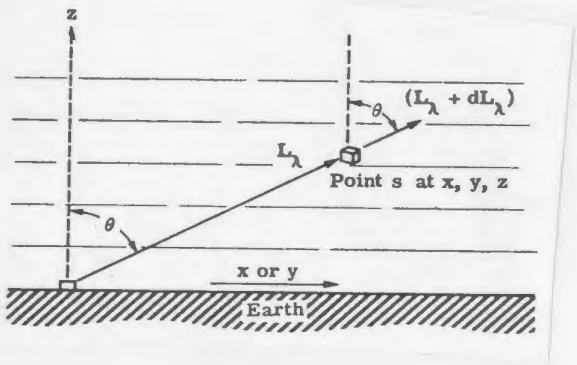

Figure 35 Radiance extinction. (Infrared Handbook, 1978)

CHAPTER 3

ATOMSPHERIC CONSIDERATIONS

3.1 Atmospheric Scattering

The solution for the radiative transfer equation for scattering atmospheres is very complex mathematically and involved physically. It is beyond the scope this report in its mathematical form and only becomes a problem after the selection of a system for making infrared measurements. When this point is reached atmospheric scattering models will be required to improve the performance of a selected instrument.

Scattering involves the extinction of radiation. It is proportional to the density of the medium and the distance through the medium which is traversed by the radiation. The relationship can be described physically in Figure 35. The sum effect is that scattering reduces the signal strength as received at the infrared instrument. This attenuation is dependent upon both molecules in the atmosphere and atmospheric aerosols. Molecular scattering follows the Rayleigh Laws and occurs mostly in the visible region. When compared with scattering by aerosols, molecular scattering is negligible. The sun's emission spectrum peaks in the

centre of the visible region and molecular scattering is considered confined to this region. Scattering by aerosols depends more on the size of the aerosol and is less dependent on wavelength. In heavy haze conditions aerosol scattering can be considered to occur in both the visible and infrared regions.

3.1.1 Aerosol Properties

Aerosols are normal constituents of the atmosphere with mass-mixing ratios near the surface varying from a few g m^{-3} in very clear air to over 100 g m^{-3} in polluted air. Aerosols may be introduced into the atmosphere as wind raised dust and sea salt, products of combustion such as soot, ash, condensed organics and products formed by chemical reactions in the atmosphere involving gaseous materials such as sulphates and nitrates. Particulates are removed from the atmosphere principally by gravitational fallout, condensation on the particle followed by subsequent rain out, and capture by falling precipitation. Residence times may vary from number of weeks in the troposphere and up to years in the stratosphere where the processes of condensation and precipitation are normally absent. To compute radiative transfer properties or the optical properties the properties of

the aerosols as well as the molecular constituents must be known.

3.1.2 Atmospheric Aerosol Models

Several models exist to describe the interaction of the atmospheric aerosols with electromagnetic radiation. The particle size distribution has received most of the attention. The resultant models are complicated and simplified models are required for operational use.

3.2 Atmospheric Absorption

Radiative transfer in the atmosphere depends on mass absorption and mass scattering. Absorption is responsible for the spectral transmittance and available radiance of the atmosphere.

The most practical approach to computing atmospheric absorption is to use an approximate, mathematically workable model of the band structure. This assumes that line positions and strengths are distributed in a way that can be represented by a simple mathematical model. The most commonly used models are:

1) Elsasser or regular model,

2) Statistical or random model.

3) Random-Elsasser model, and

4) Quasi-random model.

Two practical methods for calculating spectral transmittance are:

1) the Aggregate method, and

2) the Lowtran method.

Neither method perfectly reproduces the results of field measurements. Direct line-by-line calculations are required to achieve occurrences consistent with that of the basic data.

Certain portions of the spectrum consist of a number of lines where near total absorption occurs. The knowledge of these areas allow the selection of infrared systems for the making of measurements of different kinds.

The presence of carbon dixoide (CO_2) strongly affects the absorption and emission of atmospheric radiation. Strong radiation absorption caused by CO_2 occurs in the 2.7 μm, 4.3 μm and the 11.4 μm to 20 μm

regions. Weaker absorption bands are located at 1.4 μm, 1.6 μm, 2.0 μm, 4.8 μm, 5.2 μm, 9.4 μm, and 10.4 μm. The 11.4 μm to 20 μm region is very important in infrared studies. In this region there are several strong and medium CO_2 absorption bands. The strongest occurs centred about 15.0 μm.

Nitrous oxide (N_2O) is considered to be abundant enough to show absorption lines. N_2O absorption occurs at 3.9 μm, 4.06 μm, 4.5 μm, 7.8 μm, 8.6 μm, and 17.0μ m.

Carbon monoxide (CO) is considered to be uniformly mixed vertically up to the tropopause. Above this layer it is oxidized by CO_2. The concentration then increases higher in the stratosphere and in the mesosphere. Absorption occurs at 2.3 μm and 4.7 μm.

The volume mixing ratio of methane (CH_4) is almost 1.6 ppm and is approximately constant with altitude up to the tropopause. It then decreases rapidly in the lower stratosphere. CH_4 absorption occurs at 3.31 μm, 6.5 μm and 7.6 μm.

Water vapour (H_2O) is the atmosphere's most variable gaseous constituent from the standpoint of

atmospheric transmittance. Profiles of water vapour are regional temporal profiles due to atmospheric conditions and geographical location. Total absorption of H_2O occurs at 1.87 μm, 2.70 μm and 6.27 μm with minor absorption occuring at 9.4 μm, 1.1 μm, 1.38 μm and 3.2 μm.

Ozone O_3 is a highly variable atmospheric constituent with respect to both time of year and geographical location. The concentration peaks at about 30 km. Ozone abscrption occurs at 9.6 μm.

Measurements of atmospheric transmittance at sea level have been made by several investigators. Figures 36 and 37 show the data of Taylor and Yates (1957) over three different path lengths. These figures basically define the transmission windows for infrared radiation.

The two important factors to consider when making atmospheric transmittance calculations are what parameters affect the computation and how they vary in a given slant path. The concentration of the absorber as a function of the path and the path dependence of the absorption coefficient must be known. For horizontal path calculations, temperature and pressure are usually taken to be constant with the values

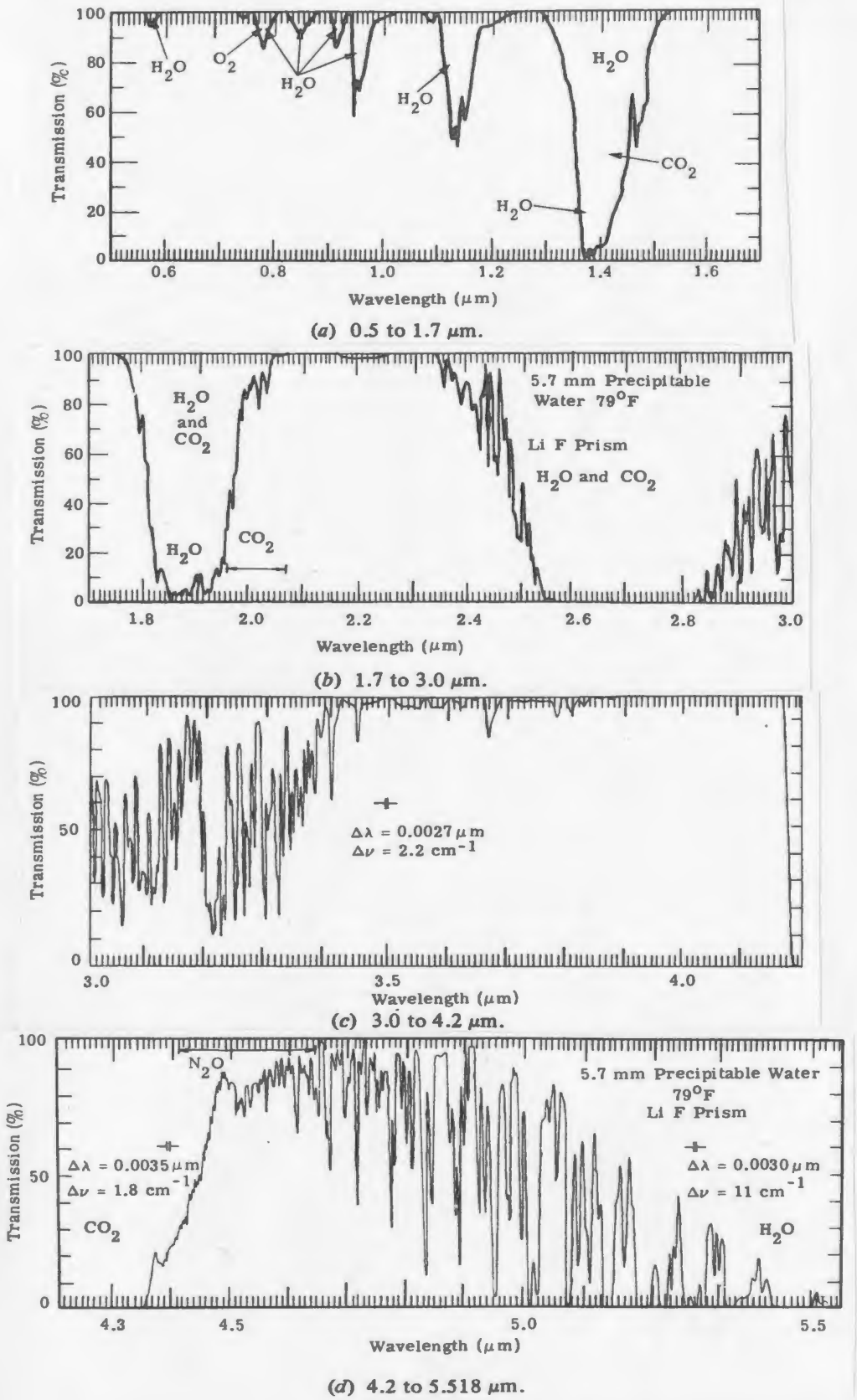

Figure 36 Atmospheric transmission at sea level over a 0.3 km path. (Taylor and Yates, 1957)

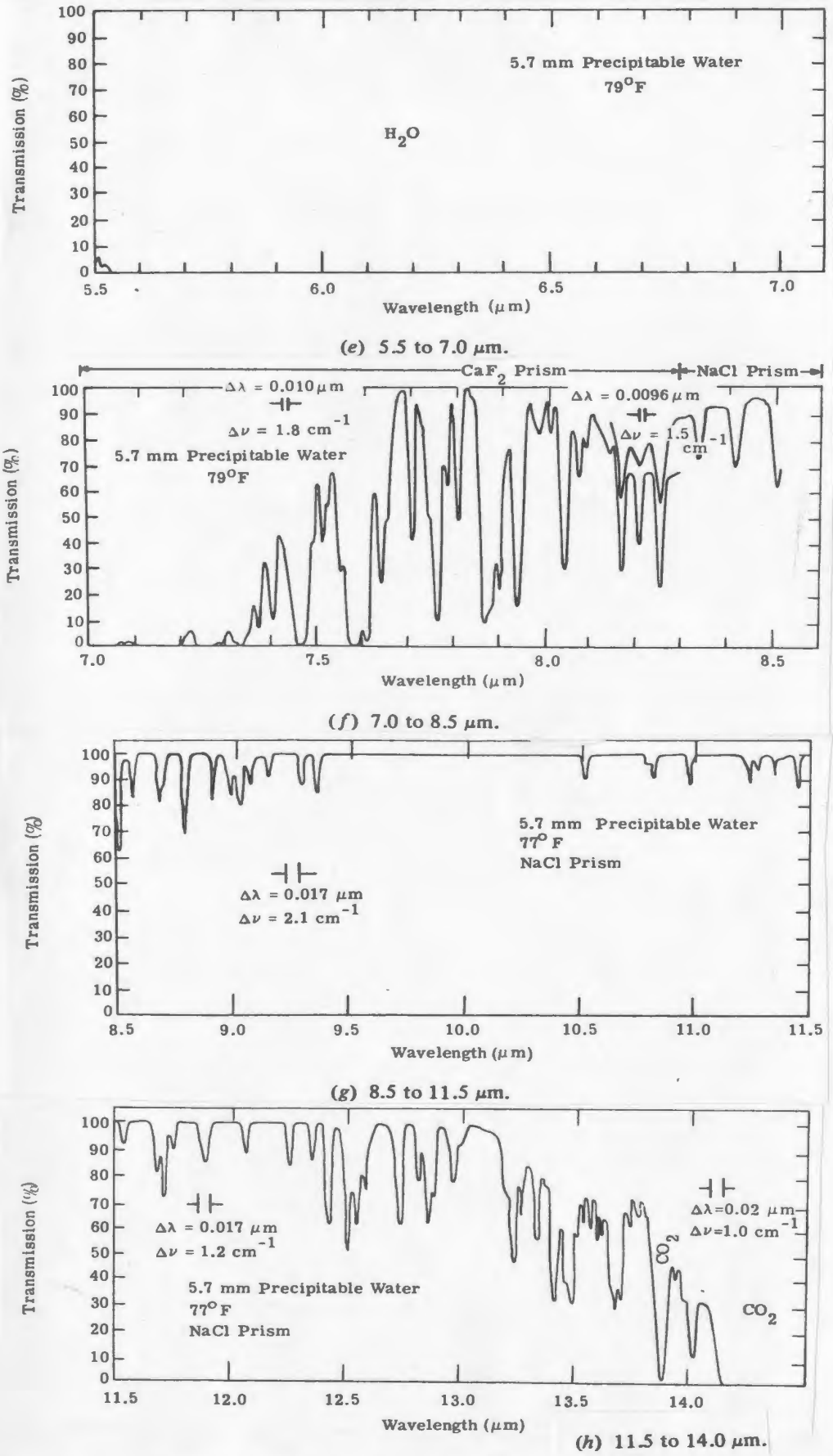

Figure 36 Atmospheric transmission at sea level over a 0.3 km path. (Taylor and Yates, 1957) (Continued)

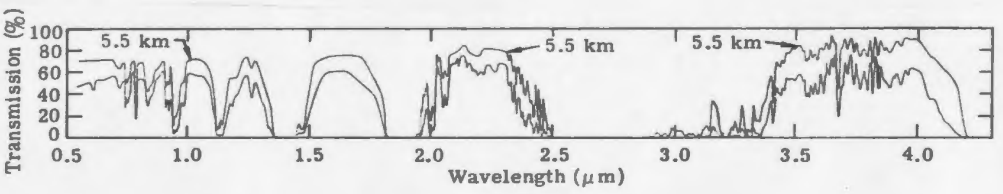

(*a*) 0.5 to 4.0 μm.

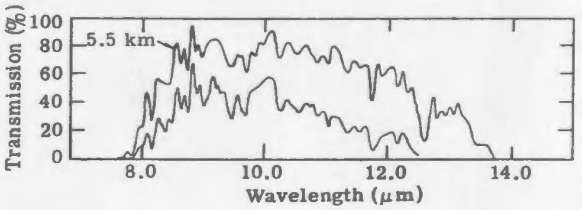

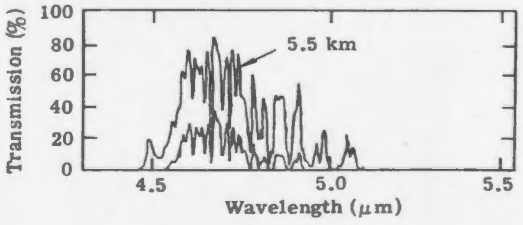

(*b*) 4.5 to 5.5 μm.

	5.5 km	16.25 km
R. H. (%)	51	53
Temp. (^{o}F)	64	68
H_2O in Path (cm)	4.18	15.1
Transmission at 0.55 μm (%)	70	43

(*c*) 8.0 to 14.0 μm.

Figure 37 Atmospheric transmission at sea level over 5.5 and 16.25 km paths. (Taylor and Yates, 1957)

measured at the presumed location of the detector. For slant path calculations the quantities are usually assumed to follow some form of a model.

The vertical distributions of particle densities for clear and hazy atmospheres are given as Table 3. The hazy model is the same as the clear model above 5 km, but increases exponentially below 5.0 km. Thus, only the lower five kilometers of atmosphere will have changing properties. Above this altitude transmission, scattering, etc. will be close to constant. Thus, the measurement scenario (section 1.2) becomes a cylinder with a height of 2.7 nm with respect to atmospheric conditions.

3.3 Other Considerations

Turbulence induces random irregularities in the atmosphere's index of refraction. These irregularities cause the optical wave fronts to become distorted. As the radiation with a distorted wavefront continues to propagate, its local irradiance also must vary under the focusing and spreading effects of the wavefront. Turbulent effects are random and complicated and are normally dealt with in a statistical framework. Distorted wavefronts are the primary cause of image

Table 3 Aerosol Models: Vertical Distributions for a Clear and Hazy Atmosphere (The Infrared Handbook, 1978)

Altitude (km)	*Particle Density, D* (particles per cm^3)	
	23 km (Visibility Clear)	*5* km (Visibility Hazy)
0	2.828E+03	1.378E+04
1	1.244E+03	5.030E+03
2	5.371E+02	1.844E+03
3	2.256E+02	6.731E+02
4	1.192E+02	2.453E+02
5	8.987E+01	8.987E+01
6	6.337E+01	6.337E+01
7	5.890E+01	5.890E+01
8	6.069E+01	6.069E+01
9	5.818E+01	5.818E+01
10	5.675E+01	5.675E+01
11	5.317E+01	5.317E+01
12	5.585E+01	5.585E+01
13	5.156E+01	5.156E+01
14	5.048E+01	5.048E+01
15	4.744E+01	4.744E+01
16	4.511E+01	4.511E+01
17	4.458E+01	4.458E+01
18	4.314E+01	4.314E+01
19	3.634E+01	3.634E+01
20	2.667E+01	2.667E+01
21	1.933E+01	1.933E+01
22	1.455E+01	1.455E+01
23	1.113E+01	1.113E+01
24	8.826E+00	8.826E+00
25	7.429E+00	7.429E+00
30	2.238E+00	2.238E+00
35	5.890E-01	5.890E-01
40	1.550E-01	1.550E-01
45	4.083E-02	4.082E-02
50	1.078E-02	1.078E-02
70	5.550E-05	5.550E-05
100	1.969E-08	1.969E-08

motion, image distortion and added blur in optical imaging systems. The distortions are also the primary cause of beam wander and added spreading when narrow beams of radiation are transmitted.

The term scintillation is used to describe the turbulence-induced random variations of local irradiance. This includes the twinkling of starlight and the speckle effects in radiation distribution at targets.

The index of refraction for the earth's atmosphere (below 40 Km) depends on temperature, pressure, humidity and optical wavelength. The effects of turbulence-induced pressure variations are negligible compared to those of temperature, or humidity fluctuations. The effect of humidity fluctuations upon the index of refraction become stronger as the optical wavelength increases beyond each major water vapour absorption band. The effect is small enough to be ignored, except in very humid atmospheres or in very critical applications. The dependence of the index upon wavelength can usually be ignored when considerating small changes of the index. Thus, with the above simplifications, index of refraction fluctuations depend only on temperature fluctuations.

The ground affects the air in two manners. First, it shears the wind through a frictional interaction with the free stream air flow and second, it serves as a source (or sink) of thermal energy which can be imparted to the air.

A typical condition would be a sunny day-time condition. In this situation the surface becomes hotter than the air thus it is a source of heat. Thermal convection takes place creating unstable or active conditions. At night the surface cools by radiation and becomes colder than the air. It becomes a heat sink with respect to the air. Convection is inhibited because the cold air stays below the less dense warm air. Thus conditions are stable or passive. If the surface and the air have the same temperature conditions a phenomenon known as pluming is associated with strong active convection. In this process the heated air rises in the form of giant bubbles or plumes and cool air descends between the plumes to replace the hot air. The turbulent temperature fluctuations in the hot plumes are greater that those in the descending cool air thus there are spatial and temporal variations in the structure parameter at the same altitude.

Changes in solar heating caused by clouds or

variations in the properties of the underlying surface also cause variations in the structure parameter.

As previously stated, scintillation is the turbulence induced randon variation of local irradiance. In many applications radiation is collected by an optical system with an entrance aperture of finite diameter. Turbulence induced fluctuation in incident radiation will result in corresponding fluctuations in total collected signal strength. If the aperture is large compared to the lateral dimensions of the irradiance fluctuations, then an averaging effect will take place. The scintillation of the total radiation from multiple independent sources will be less than the scintillation from a single source because of averaging effects.

Image degradation occurs if there is turbulence in the optical path. The image becomes distorted if parts of an image move in relation to other parts of the image or if the image becomes blurred. The distortion can be so great that the image appears to be broken up. Effects of distortion depend on how long the sensor or detector is exposed to the target. The length of exposure affects the degree of degradation. Too short exposure will result in not enough time to register a

target. Too long exposure can cause a blurred image.

A phenomena called crossover can also cause problems. At certain times during the diurnal heat cycle of the background a point is reached where the temperature of the background and the target are the same. This condition, however, does not necessarily apply to the entire target cross-section and detection may still be possible.

CHAPTER 4

INRARED COMPONENTS AND SYSTEMS

4.1 System Description

An infrared system consists of many components each with characteristics that must be known and understood if they are to be utilized. A required component integration can be seen in Figure 38 which is a block representation of a basic infrared system.

The purpose of the optics is the collection of the radiation that is being sensed. The design of the optical system is dependent upon the requirement of the infrared system. The scanner consists of an optical section which collects the radiation and focuses it on a detector. The detector converts radiation into an electrical signal which is then displayed or recorded. Attached to the detector is some form of a cooling system which lowers the detector's temperature in order to increase its sensitivity.

Some functions of the basic system can be integrated into an image tube system (Figure 39). In this type of system the imaging tube acts much like a television camera. The imaging tube is a self-contained optics - scanner - detector system. It

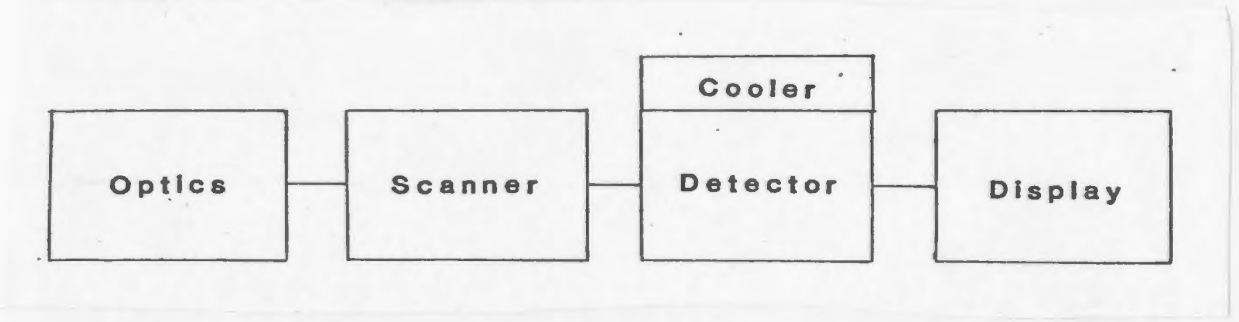

Figure 38 Basic Infrared System Block Diagram

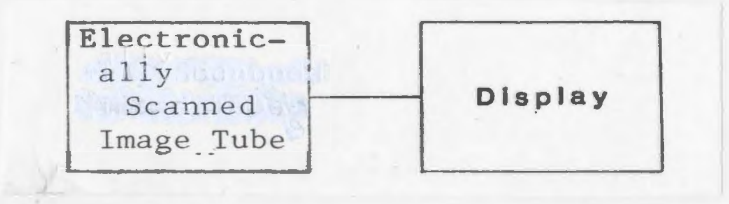

Figure 39 Basic Infrared Block Diagram Where the Imaging Tube Replaces the Optics, Scanner and Detector

detects temperatures that are the same or hotter than the temperature of the detector.

4.2 Optical - Mechanical Scanning Techniques and Devices

Scanning devices project a small portion of the total field of view onto a detector. Many different scan patterns can be utilized and there are several different techniques that can be used to imprint the scan patterns onto the detector. These techniques involve the use of different combinations of mirrors, lenses or prisms with different driving mechanisms.

Important parameters of the various scan techniques include scan rate, scan rate constancy, scan efficiency, optical efficiency and vignetting (i.e. image uniformity). Several factors affect the scan rate and hence the constancy and the efficiency. These include the forces generated; the material strength; size and weight; and lever arm; the windage and the frictional heating.

When using a mirror scanner, the system window and the mirror being used must be larger than the diameter of the optical system entrance aperture. If this

condition is not satisfied then vignetting (signal degradation) will occur. This is especially important in framing systems such as forward looking infrared devices. In these systems the problem is two-dimensional and often requires the use of dual scanning motions.

4.3 Detectors

The detector converts the incident radiation into an electrical signal which is fed to a display. There are two basic detector classes: thermal detectors and photon detectors. The thermal detector is sensitive to incident radiation temperature and types used include; bolometers, thermovoltaic devices, thermopneumatic devices and pyroelectric devices. The photon detector measures the number of photons in the incident radiation. The basic types are: photovoltaic, photoconductive, photoelectromagnetic and photoemissive.

4.4 Cooling Systems

Cooling systems are necessary for the operation of infrared devices. They are designed to attain and maintain a desired temperature in the detecting system. There are four basic cooler categories:

1) Open-cycle, expendable systems,

2) Passive radiators,

3) Close-cycle, mechanical-refrigeration, and

4) Thermo-electric coolers.

The liquids used are called cryogenic fluids and are available for temperatures ranging from 4.2 to 240.0°K.

4.5 Optics and Optical Systems

Depending upon the complexity of the infrared sensor, the optics used can be a very simple telescope up to a complex system of reflective and refractive components. There are almost as many optical designs for infrared systems as there have been infrared systems. Optical design deals with the lenses and mirrors and their combinations which are used to build an optical system. The finer points of design are beyond the scope of this report.

4.6 Imaging Tubes

Imaging tubes are a combination of optics, scanner and detector used for infrared sensing. They are similar to television camera tubes. The generic name of these tubes is the vidicon. Systems include:

1) silicon diode array vidicon,

2) plumbicon,

3) pyroelectric vidicon, and

4) other tubes (of historical interest).

The pyroelectic vidicon is the tube in most use for infrared sensing. Its sensitivity can extend to the far infrared region out to 8 to 14 μm.

Pyroelectric vidicons form a thermal image of a stationary scene. Because pyroelectric systems respond only to changes in temperature the vidicon must be panned or chopped before the image and its changes can be seen. There have been some problems in the developement of these vidicons but most have been overcome and the devices can resolve small temperature differences from short ranges.

4.7 Display

It is not possible in this brief report to go into detail on all available CRT displays that are available for IR systems. The display normally depends on the use of the sensor. Types of displays include high-brightness CRTs for use on pilot's helmets. Short-persistence CRTs with high brightness are used

for television displays. Long-persistence CRTs are normally used for air-to-air and air-to-ground radar and IR displays but disadvantages include; low brightness, fixed persistence of image, non-linear persistence and no selective erasure. Ideally, a combination of displays is required as shown in Figure 40. Future systems may require interactive displays so that image processing techniques such as contrast stretching, edge enhancement and registration can be carried out.

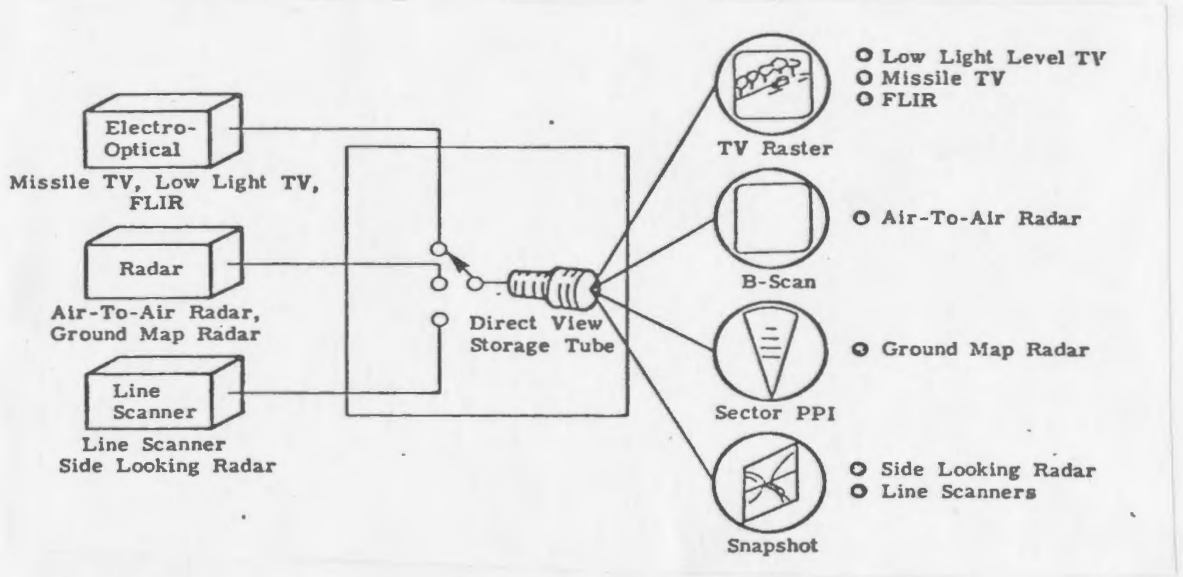

Figure 40 Multi-sensor display system using a direct view storage tube. (Infrared Handbook, 1978).

CHAPTER 5

TARGETS

Very little information is available on icebergs as infrared targets. More information is available on the infrared sensing of sea ice but very little of this is quantitative in nature. The information that is available has been recorded vertically from the air looking downward to the ground. No information has been found for measurements in the horizontal.

5.1 Icebergs - Field Data

In 1972 one iceberg was ground-truthed off the Labrador coast (Bajzak, 1974). Ground truthing was accomplished with a Barnes PRT 5 radiation thermometer. This resulted in the following, uncorrected for atmospheric path, temperature recordings.

Iceberg Surface	$-3^{o}C$
Water Surface at Iceberg Edge	$0^{o}C$
Water Surface 1000 feet from Iceberg	$+3^{o}C$

Infrared line scan images obtained from an altitude of 160 meters show the presence of a temperature envelope

around the iceberg. Digital analysis also showed the envelope. Density contour maps were generated of the temperature regime around the iceberg. Because the infrared line scanner used was nonquantitative and operated with automatic gain control the temperature data could not be correlated with the limited ground truth data.

This study was useful in that it showed a temperature contrast between the iceberg and surrounding water and a water temperature envelope around an iceberg. This example is one of several conditions that will be encountered in iceberg hazard detection using infrared. This condition was a melting state. Other expected states will be equilibrium, rapid deterioration and conditions where the water around the iceberg has commenced freezing. Superimposed upon these conditions will be back-grounds of sea water, atmosphere and a combination of both.

5.2 Ice Floes-Field Data

There is little data on sea ice and ice floes that is quantitative. Most infrared scanner data has been collected using systems without blackbody

reference sources. Automatic gain control (AGC) has normally been used to produce a pleasing infrared image that shows good contrast or differentiation between regions of different temperature. AGC gives no information about the actual temperature or radiance of the floe.

Data recording in the Straits of Belle Isle, Newfoundland in 1976 used a quantitative infrared line scanner (Worsfold and Strong, 1977). This study showed that sea ice and shorefast ice could be classified into temperature ranges. New ice and frozen slush; the outlines of floes and ice floes; shorefast and rafted ice; and snow covered ice could all be distinguished with temperatures ranging from $-4^{o}C$ to $-14^{o}C$. It should be noted that data was recorded during a period of freezing (i.e., air temperatures of the order of $-5.0^{o}C$ to $-20.0^{o}C$) and that cold temperatures prevailed over a long period of time thus the ocean water was cooled to $-1.8^{o}C$, its freezing point. This would result in heat flow from the warmer water to the colder atmosphere.

Other conditions which were not specifically studied in the Newfoundland Program were equilibrium between the air and water and conditions where the ice

was melting. This last condition was sampled near Cartwright in April 1976 and the melting conditions resulted in water on the ice which attenuated the infrared return. No quantitative results were obtained from this sampling.

From these two studies it can be seen that ice floes can be very cold or relatively warm in comparison with the surrounding water thus different target detection conditions will exist. These different target conditions will result in different infrared signals being sensed thus atmospheric and oceanographic conditions must be monitored.

5.3 Comments

Based on literature searches for target information there is a severe shortage of quantitative data on the infrared return (both temperature and radiance) of icebergs or sea ice and its different forms. When compared to basic data on the transmitting medium (atmosphere) and on the recording device (infrared system) this is the weak point in the development of an ice hazard detection system. Until more information on target infrared return is gathered selection of a suitable detection system is not feasible. A program of infrared signature analysis will require a ground

truthing program which records both oceanographic and atmospheric data both of which affect the infrared signature.

CHAPTER 6

DISCUSSION

6.1 Temperature Range of Ice Hazard Targets

To select the temperature ranges for the detection of ice hazards it is necessary to determine a range of temperatures for the targets and for the backgrounds. The background for a target looking, vertically down from an aircraft or satellite will be the surface of the earth which will be either the ocean, an ice cover or a mixture of ice and ocean for ice hazard dectection problems. Horizontally from a surface platform such as a ship, the background will be the horizontal sky, the near surface, sea ice or a combination of these components.

Using the quantitative data obtained from infrared radiometer studies (Bajzak, 1974), a surface temperature of $0^{o}C$, the melting point, is a good approximation for icebergs. From the start of an iceberg's voyage, from the time it calves from the glacier to the point where it deteriorates, the iceberg is either in equilibrium with its surroundings or deteriorating. Surface temperature will be in the range of melting or $0^{o}C$. Surface water may be slightly

higher in temperature because it is melting. As the freezing point of sea water is about $-1.8^{o}C$ the equilibrium temperature range of the iceberg surface would be the same. Therefore, it is reasonable to assume the iceberg surface temperature is in the range -2 to $0^{o}C$. Using an emissivity of 0.9 and the accuracy range of $\pm$ $0.5^{o}C$, (Barnes, 1975, Manufacturer's Specifications), Bajzak's (1974) reading of $-3.0^{o}C$ for the iceberg surface is reasonably close to the melting point range of ice, -2.0 to $0.0^{o}C$. This does not make use of atmospheric correction procedures which would be especially important for aircraft sensing (Worsfold, et al, 1977, Worsfold and Sparkes, 1977 and Wedler and Worsfold, 1979).

The values presented by Bajzak (1974) for the water envelop around the iceberg plus iceberg surface area was $-3^{o}C$ to $+3^{o}C$. This water temperature was a local condition for the area where the iceberg was measured. As sea ice freezes at $-1.8^{o}C$ this is a fixed lower limited for the sea water background. On the Grand Banks temperatures can be as high as $16^{o}C$ to $20^{o}C$ (Ketchen, LaViolette and Worsfold, 1977).

Once sea ice freezes it will make a background contribution. In a quantitative infrared study by

Worsfold and Strong (1977) in the Strait of Belle Isle, sea ice and snow covered ice showed temperatures of $-15^{o}C$ to $0^{o}C$ for blackbody recordings. Using these values as approximate limits the possible temperature range of sea ice background could be -20^{o} C to $0^{o}C$.

Figure 11 shows the radiance and temperature ranges of a cloud as observed from the surface. The temperature range is from $-10^{o}C$ to $+10^{o}C$. With the presence of the sun and no clouds the sky temperature could be measured as high as $40^{o}C$ horizontally from an observation platform (Infrared Handbook, 1978). In the regions where icebergs occur, surface air temperatures of approximately $20^{o}C$ are the normally expected highest temperatures. Therefore, the ambient temperature range in an area where icebergs occur could be $-10^{o}C$ to $+20^{o}C$.

From this discussion, it can be seen that a temperature range of $-20^{o}C$ to $+20^{o}C$ is a reasonable assumption to make for temperatures to be sensed for both target and background temperatures.

6.2 Calculations from the Basic Laws

The basic laws as outlined in Chapter 2 can be

used in determining the feasibility of using infrared devices for ice hazard detection.

The Stefan-Boltzmann Law can be used to calculate Table 4. This gives radiance limits for the conditions that would be encountered based on the discussion in Section 6.1. Wien's formula gives Table 5 and shows that for the assumptions made the spectral range 9.89 μm to 11.45 μm is the region of maximum radiation for iceberg and sea ice targets. This region is the far infrared region (Figure 2).

Planck's Curves (Figure 4) show that for 0^{o}C (273 ^{o}K) the range centred on 10 μm is the region of maximum radiation for the assumptions made. These curves show agreement with both the Wien and Stefan-Boltzmann calculations.

Using the GEN-15-L Radiation Calculator (a special slide rule based on the Planck Equations) the results of this section are quickly confirmed. This calculator gives more precise values than Figure 4 and is normally used for everyday calculations.

These simple calculations show that for the assumed temperature range maximum radiation is emitted around 10.6 μm.

Table 4 Calculations Using Stefan-Boltzmann Relationship (Radiance calculated in W/cm^2 for different temperatures and emissivities)

(emissivity)	T (^oK) A 253	B 273	C 293
0.1	2.32×10^{-3}	3.15×10^{-3}	4.18×10^{-3}
0.2	4.64×10^{-3}	6.30×10^{-3}	8.35×10^{-3}
0.3	6.97×10^{-3}	9.44×10^{-3}	12.53×10^{-3}
0.4	9.29×10^{-3}	12.59×10^{-3}	16.71×10^{-3}
0.5	11.61×10^{-3}	15.74×10^{-3}	20.89×10^{-3}
0.6	13.93×10^{-3}	18.89×10^{-3}	25.06×10^{-3}
0.7	16.25×10^{-3}	22.04×10^{-3}	29.24×10^{-3}
0.8	18.58×10^{-3}	25.18×10^{-3}	33.42×10^{-3}
0.9	20.90×10^{-3}	28.33×10^{-3}	37.59×10^{-3}
1.0	23.22×10^{-3}	31.48×10^{-3}	41.77×10^{-3}

Table 5 Wien Calculations

$\lambda T = K = 2897.9$ micrometer degrees

T (^{o}C)	T (^{o}K)	λ (micrometers)
-20	253	11.45
0	273	10.62
20	293	9.89

6.3 Emissivity

Using the GEN-15-C Radiation Calculator the effects of emissivity changes can be assessed. Testing for emissivity ranges of 0.10 to 0.99 it can quickly be shown that the assumed conditions of natural temperatures (273 $^{o}K(0^{o}C)$) give an emissivity range of 0.7 to 1.0 for various types of sea ice. These values are in agreement with published references (Mueller et al, 1975, The Infrared Handbook, 1978).

6.4 Other Radiation Laws

A Lambertian surface is a surface defined as one whose radiance is independent of the angle of viewing. Another way of saying this, is that, the radiant exitence is the same in all directions. A smooth flat surface or a smooth regular curved surface would approximate a Lambertian surface but some types of icebergs because of their size/shape relationships could not be expected to be Lambertian in nature. Therefore, the radiance from many ice hazard targets because it is coming from a non-Lambertian surface will vary thus a target will give different readings from different look directions.

Because an emissivity of 0.7 to 1.0 can be expected from an ice target then it can be said to be a reasonably good radiator which in turn implies that they are also good absorbers. This implies that for a period of time after the radiation source is removed emitted radiation will continue until only a passive radiation is emitted. At lower latitudes, an ice target will emit radiation at night or in overcast conditions. Without considering other sources of thermal power, ice targets will be detectable for periods other than during day time heating. After the absorbed radiation is emitted the passive or inherent thermal radiation will produce a signal.

6.5 Backgrounds

6.5.1 Sky Radiation

Figure 6 shows that the spectrum can be divided into regions of solar scattering and thermal emission. Solar scattering is predominant in the middle infrared region. Thermal emission is prominent in the far infrared region. Figure 7 shows that as the temperature increases the spectral radiance increases with a peak centered around 10.6 μm. Figures 8 and 9 show that regions with strong absorption and hence emission approach the blackbody curve appropriate for

the temperature of the atmosphere. Less strongly emitting regions contribute only in a minor way. These figures show that boch the 3 to 5 and 8 to 14 μm bands have potential use. The data does not show elevation differences for the 3 to 5 μm region. These curves show that attenuation decreases with increasing elevation angle from the horizon. The curves also shows a small region around 9.6 μm where attenuation increases relative to the surrounding wavelengths.

Figure 10 shows that in the 3 to 5 μm region scattered radiation affects the radiance in a variable manner while emissive radiation begins to have an effect. Cloud cover effects in Figure 11 show a direct relationship between higher radiances under no cloud conditions to lower radiance with cloud conditions. Figure 12 shows that emission under cloud cover varies with increasing elevation angle from the horizon. Figure 13 shows that there are seasonal emission variations.

These results show that several conditions affect the absorption and hence emission of the sky and thus the emission of the background sky radiation varies. More emission will occur at the horizontal than at the vertical look angle and when there are strong

absorption bands strong emission will also occur. They show that the prime sensing region will be centred about 10.6 μm.

6.5.2 Marine Backgrounds

Because water is opaque to infrared radiation at wavelengths longer than 3 μm, the 0.01 cm (Figure 29) surface layer determines the radiance of the water. Surface water temperature will influence the water background of a sensor for detecting ice hazards. Figure 18 shows that there will be a great deal of reflectance from water in the 3 to 5 μm region and a comparatively small amount in the 8 to 14 μm region. Figure 20 shows that reflection increases as the angle of incidence increases and Figure 21 shows that while reflectance goes to a maximum as angle of incident increases, the emissivity of the water decreases as the angle of incidence is increased. The absorption of infrared radiation by water is a maximum at 3 μm while values are high around 8 to 10 μm. This shows that reflectance will be much greater in an aircraft mounted system than in a ship mounted system.

As the roughness of the sea surface increases the radiance will increase (Figure 24) and overcast skies

result in decreased radiance (Figure 25) for rough seas. Rough sea effects can also be seen in Figures 26, 27 and 28.

Using Figure 29 it can be seen that sea surface temperature contributes to the total radiance of the sea. Currents and temperature anomalies will thus produce radiance anomalies. In summary, it can be seen that the changing conditions of the sea will result in changing background radiance in ice hazard detection. These changes will be more pronounced for an aircraft mounted sensor looking down than for a ship mounted sensor looking across the water surface.

6.5.3 Sun, Snow and Earth Backgrounds

The effects of the sun can only be shown for the visible and near infrared (Figures 30, 31, 32 and 33). The irradiance decreases at sea level versus outside the atmosphere. There is a lack of data at the middle and far infrared wavelengths but Table 1 shows that sun effects can be considered low especially as the wavelength increases toward the far infrared.

The lack of data in the literature on snow precludes any statement concerning its effect

especially in the 8 to 14 μm region. Thus, snow cover on ice could be a problem that may have to be dealt with.

The most important aspect to relize about the irradiance of the earth is that it results in diurnal variations that change the radiance measured. These variations are due to solar heating and will have some effect especially on wide bandwidth detectors.

6.6 Atmospheric Scattering

Rayleigh or molecular scattering greatly affects the visible portions of the electromagnetic spectrum. The effects of molecular scattering decrease toward the near infrared and there is very little affect in the far infrared. Aerosol scattering increases from the visible toward the far infrared. This type of scattering is called Mie scattering. The only method to quantitatively deal with aerosol scattering is to determine the aerosol size/diameter distributions and then determine their influence on scattering by using atmospheric aerosols models. Very little data is available about marine aerosols as they are difficult to measure. These aerosols in the form of sea spray may cause some problem with target detection

especially at longer ranges.

6.7 Atmospheric Absorption

Because certain portions of the spectrum contain many absorption lines due to different atmospheric constituents some portions of the infrared spectrum will totally block the transmission of infrared radiation while other areas act as windows and infrared transmission can be as high as 100%. Figures 36 and 37 show the transmission and absorption regions for the three different ranges. It can be seen that there are several transmission windows in the middle infrared with the most important being the region from 3 to 5 μm. In the far infrared region the most important window is the 8 to 14 μm window. Within each of these windows there are some spectral regions where atmospheric absorption occurs due to a particular atmospheric constituent.

An examination of these data show that within 3 to 5 μm region there is a major absorption band around 4.3 μm that breaks this window into two and that from 3.0 to 3.5 μm and from 4.6 to 5.0 μm there are several absorption bands that could cause signal attenuation. In the 8 to 14 μm window there are also several

absorption bands but the region from 9.6 to 11.5 μm show almost 100% transmission. This coincides with the optimum wavelength of 10.6 μm from the radiation laws. These figures also show that transmission reduces with an increase in range.

Because of the wide transmission pass band in the 8 to 14 μm region and because it is the prime potential region for infrared ice hazard detection selective narrow pass band filters can be used over several portions of the region. This will allow for flexibility in detection and could be valuable if sea ice has its peak signal in a different part of this range than ice bergs.

In summary, it can be seen that there are two important transmission windows where infrared sensing can be carried out, the 3 to 5 and the 8 to 14 μm regions. Because some absorption occurs in these regions special filters can be used to reduce the effects of this attenuation and to reduce detection bandwidths.

6.8 Other Phenomena

6.8.1 Turbulence

Turbulence near the ground results in ground effects which can produce thermal anomalies and thus radiance variations in the total viewed scene, both target and background. Turbulence in an optical path can blur an infrared image scene and/or it can distort the spatial aspects (i.e., portions of images can move in relation to other portions) resulting in a broken image. Scintillation is another affect of turbulence. The turbulence induces fluctuations in the incident radiation which results in fluctuations in the total collected signal strength. Scintillation is reduced by aperture averaging (a large aperture compared to the lateral dimensions of the fluctuations).

6.8.2 Crossover

A particular condition exists that can affect the recording of infrared target data. This is called crossover and occurs at the time of the day when the atmosphere and the targets are the same temperature. This is normally in the early morning and early evening when the atmosphere is either warming up to its maximum or cooling to its minimum. At this time

detection of ice hazard targets may be difficult if the atmosphere approaches the temperature of the targets. The crossover point is different for different targets and different atmospheric conditions, thus sea ice targets may be affected at a different point in time than an iceberg target.

6.9 Spectral Regions

As can be seen from Figure 1 there are three infrared regions that could be utilized. The near infrared region is also called the photographic region. In this region photographic devices are used to record the infrared data available. In this region it is the solar reflected light that produces the signal. Thermal effects do not contribute to the sensed signal in this range. The middle infrared region senses both solar reflected and thermal infrared data while the far infrared energy is produced thermally by molecular motion. Section 6.7 deals with these regions in detail but it should be noted that each region would require completely different types of sensor systems.

6.10 Infrared Systems

As can be seen from the information presented in

Chapter 4, infrared systems can be highly variable. This is the result of systems being developed as prototypes or one of a kind for special applications. The variety of infrared systems can be compared with the variety of optical systems in the visible spectrum (i.e., binoculars, cameras, telescopes, televisions, and optical range finders). This is because the same principles of geometric optics apply in both cases. In regards to detectors, they are the "eye" counterpart in the infrared region. The cooling systems are required to make the eye operable and the scan techniques make the eye functional.

There are two families of potentially suitable infrared systems. One of the families can be divided into two subclasses. The pyroelectric vidicons are one of the two families. Their counterpart in the visible are binoculars, telescopes and television cameras. The pyroelectric vidicon has always been used to extend visible systems into the infrared regions thus ordinary binoculars become night vision binoculars and low light level television cameras extend into the infrared region by way of the commonly known pyroelectric vidicon. Because of the detectors and cooling systems being used, these infrared devices are short range systems, present state of the art. New advances in solid state electonics especially in

charge coupled devices show a promising potential for improved future systems, in resolution and detectability, but present off-the-shelf systems do not appear to have the potential. Pyroelectric vidicons have never been used for ice hazard detection.

The second family includes the Forward Looking Infrared Systems (FLIRS) and the infrared television. The difference is mainly in the nomenclature. FLIRS are infrared systems which use scanning machanisms in the optics system and detector systems that are cooled to a very low level. These systems are related to airborne infrared line scanners used in remote sensing aircraft successfully at altitudes of 45,000 feet. These systems show great promise in infrared ice hazard detection. They are military devices that are currently being used for detecting military targets such as tanks, which are comparable in size to growlers. The major problems with FLIR devices are the military classification, the requirement for gyrostabilization for operation and the lack of target data. Infrared television systems, besides being similar to FLIRS, have developed analog and digital packages that make the sensor useful as a target signature characterization tools. They can be used to obtain the necessary information that is presently

lacking about the various ice hazards that must be detected.

6.11 Specifications for Thermal Imaging Systems

The end goal of the infrared portion of the ice hazard detection program is to obtain the required target data so that design criteria and specifications can be developed for an operational field system. It is recognized by this study that this can only be achieved after target data is available. A sample specification outline can be developed at this time so that the field technical plan can be developed in a manner which will collect field data in the most economical and beneficial way.

The primary performance parameters which are required at the end of the target signature phase include:

1. total field of view (TFOV) (spatial resolution)
2. pointing range (of the centre of the TFOV) (spatial resolution)
3. signal transfer function in terms of λ and T (spatial frequency and thermal resolution)

4. minimum resolvable temperature (as a function of angular spatial frequency)
5. dynamic range
6. reference level range
7. frame rate
8. forward velocity/range capability
9. rate of information update
10. size, type, luminance, viewing distance and apparent magnification of display.

In addition to the primary parameters there are several secondary performance paramenter that may have some bearing on the final specifications. They include:

1. static uniformity as a function of scene temperature
2. moving patterns
3. geometric distortion
4. image stability
5. optical noise
6. blemishes in image
7. scan pattern
8. display spectrum

Several other characteristics will require definition before a ship mounted system can be

specified. These characteristics include:

1. size and weight
2. power consumption
3. gyrostabilization requirements
4. mean time before failure
5. maintenance levels
6. test features
7. environmental requirements
8. minimization of indicators, switches, dials and knobs
9. capability of constant operation
10. standby mode
11. detector quality
12. cooling requirements
13. display requirements
14. human interface and human engineering

6.12 Discussion of Scenario

In Section 1.2 a scenario was developed to place in context the use of infrared sensors to detect and monitor ice hazard targets. In review, the scenario defined a cylinder 22nm in diameter and 6nm in height around a stationary drilling platform or ship. The scenario defines the reference frame for the operation of the infrared system. By defining this reference

frame the sensing of ice hazard targets can then be restated in engineering terms and hence becomes a complex transmission problem.

The ice hazard becomes the passive source of the transmitted signal or target irradiance. The infrared sensor becomes the receiver of the signal and the intervening atmosphere and the problems it imposes becomes a selective filter.

The transmitter (ice target) produces a signal which is a function of the target temperature and its spectral emissivity. The temperature depends on several factors which include solar heating, thermal melting and other factors of radiative heat transfer. The spectral emissivity is a function of the target material (ie. fresh or salt water) and surface roughness (ie. degree of smoothness and target age). Because the energy is from the target itself the energy is passive. The changing state of the ice target (ie. melting, rotation, aging) produces variations in the transmitted signal. Thus, signal level is not a constant.

The infrared sensor is the receiver. It records and measures the transmitted signal. The receiver can

be characterized by its modulation transfer function (MTF) which is a measure of the resolution of the electro-optical receiver (Brock et al, 1965; and RCA, 1974). The MTF is a sine-wave spatial-frequency amplitude response. The MTF is useful in that the major components of the infrared system each have an MTF and these can be cascaded so that an overall system resolution can be measured. Thus, if the MTF for each component, lens, aperture, pass band filter, scanning optics and detector can be written as a sine-wave response then the system MTF and hence a measure of receiver resolution can be achieved by multiplication of the individual MTF. It should be noted that the radiation measured from the target will be in that portion of the electromagnetic spectrum for which system sensitivity has been designed.

The intervening atmosphere can be regarded as a selective filter. The filter characteristics will be dependent upon the conditions that occur during the real time operation of the receiver. Atmospheric conditions such as humidity, scattering, and temperature will change the filter characteristics.

Sources of noise complete the problem definition. These sources can come from the target (ie. thermal

deterioration), the atmosphere (scintillation, crossover, turbulence), and/or the receiver (detector noise, electric noise, mechanical noise from the scanner). In addition, the target backgrounds, the sky, the sea and/or terrain such as a mountain or coastline must be considered as noise sources as the detection of the ice target is the problem. In other circumstances these backgrounds would be targets and in the final solution to the ice hazard detection problem these backgrounds may have to be considered as both signals and noise.

Therefore, the transmission problem can be stated in terms of the target to background ratio at the viewing device. This is not precise but the simplified target to background ratio is easily measured using various infrared instruments and is the logical first measure of any system used. The target to background ratio must be extended by including the system effects. Once system effects are considered then the problem can be stated in terms of the signal to noise ratio which then allows for the development of true target characteristic signatures and the ability to evaluate any infrared sensor using the signature and the particular system effects.

Once characteristic signatures are achieved for a

particular set of physical and environmental situations they must be extended and extrapolated in terms of the scenario developed for this report or for any other suitable scenario.

This means that if a target is detected in the scenario cylinder then its range and azimuth to either the ship platform or aircraft platform must be evaluated in terms of how the data for the recorded position might change if it were located in a different portion of the scenario cylinder. The recording of a number of targets will assist in the development of the required data base to assess this portion of the total problem.

In summary, the problem of infrared detection of sea ice hazards can be defined as a transmission problem and reduced to simplified target to background ratios and extended to signal to noise ratios when system and environmental effects are included. If data were collected in a field program then the signal to noise ratios obtained would be analyzed and system characteristic target signatures could be developed in terms of the system used. The removal of system effects would result in characteristic target signatures which would be "true" target to background

ratios. These "true" signatures could then be assessed in terms of the geometry of the scenario cylinder and the environmental changes that can occur within the scenario area. Then, any sensor system, of which the system effects are known, could be evaluated using the "true" characteristic signatures. By the application of spatial and time shifts the stationary platform becomes a moving vessel and the aircraft would cover a wider area providing coverage over a greater distance in advance of a moving vessel. This extended scenario area would then include close-tactical, tactical and strategic requirements for infrared ice hazard detection for a complete area, say for example the Labrador Sea. This extrapolation could then be used for ice hazard mapping.

Once the "true" characteristic signatures, have been achieved then meaningful relationships such as minimum resolvable target size with respect to range can be developed. For example, it would be expected that all icebergs would be detectable at any location within the defined detection envelop and the smaller targets such as ice floes would be size and resolution limited and could only be detected at the near ranges.

CHAPTER 7

SUMMARY, RECOMMENDATIONS AND CONCLUSIONS

7.1 Summary

The absorption regions of the infrared spectrum define two potential areas where it may be possible to detect ice hazard targets using sensing systems that operate on infrared principles. These regions are defined by the absorption of different constituents. The two windows are the 3 to 5 μm region and the 8 to 14 μm region. The 3 to 5 μm region is not entirely clear and is broken by major narrow absorption bands. The 8 to 14 μm region is basically clear except for a major absorption band around 9.6 μm. For all intents and purposes the 8 to 14 μm region is clear in the region 9.6 to 11.5 μm, with 100% transmission capability. Therefore, infrared sensors will have to operate in one of these two bands to detect ice hazards based on the thermal properties of the hazards.

Within these two bands the sky and marine backgrounds can be characterized. Because only the surface of water bodies determines radiation

properties, the surface temperature distribution will have the greatest effect due to the marine portion of the background. Sea state conditions can alter the temperature pattern by lowering the emissivity and oceanographic upwellings can change the surface thermal pattern. For a sensor operating from a ship the sea state will probably have the greatest effect mainly due to emissivity changes. For an airborne system, upwellings and current interchanges will change the surface thermal pattern in the target area. The thermal envelope around the ice target will have minimal effect on radiation received by a ship mounted sensor because of the low look angle. For an aircraft sensor the envelope around the ice target could potentially under some circumstances make the target look larger than it actually is. Reflection from the water surface will be greater in the 3 to 5 μm region but this will only effect the vertical looking aircraft sensor.

The sky background shows infrared emission in both the 3 to 5 μm and 8 to 14 μm windows. As gas constituents are in the atmosphere and cause absorption bands they can attenuate radiation within these windows. Close examination of this effect shows that the 3 to 5 μm region is actually broken into

several smaller windows. The edges of the 8 to 14 μm region receive some attenuation but the central portion of the window is essentially 100% transmission. More attenuation occurs over the horizontal path than the vertical path because of the "thicker" atmosphere over the horizontal. This attenuation will have a more pronounced effect on the ship sensor than the aircraft sensor. Solar scattering occurs in the 3 to 5 μm region which adds an attenuation factor to this window that is highly variable. Because the 8 to 14 μm window has a wider clear passband more variety in spectral filtering is possible, this of course will be dependent on the peak transmission wavelength of the targets. Filtering in the 3 to 5 μm region will be mainly to reduce solar scattering and eliminate absorption bands. A major factor in the sky background radiation will be the ambient air temperature and humidity. Humidity increases will tend to increase attenuation. Air temperature is a highly significant variable because of diurnal heating and cooling as well as vertical and horizontal movement of air masses. Sun angle is expected to only be a factor in diurnal heating, otherwise the infrared system is a total day-night sensor.

The distribution of aerosols in the atmosphere

depends on humidity, particle size, and concentration of particulates. Rayleigh scattering will have some possible effect in the 3 to 5 μm region but not in the 8 to 14 μm region. Mie scattering occurs in the 3 to 5 μm region and increases with increasing wavelength. Depending on the particle size distribution severe attenuation due to Mie scattering could occur in the 8 to 14 μm region. Atmospheric modelling will be required to assess aerosol effects.

It has been shown in this report that a temperature range of $-20^{o}C$ to $+20^{o}C$ is a reasonable assumption for the infrared sensing of ice hazards on water or sky backgrounds. Experimental data available shows that the ice targets would have temperatures that fall in the middle of this range thus the potential for detection is high. At the same time, because of temperature similarities, problems such as crossover could be encountered. The whole problem of ice hazard detection fall within ambient naturally occuring temperatures.

Using the basic laws of radiation and performing simplified calculations it can be seen that wavelengths, radiative power, expected temperatures and emissivities can be determined. The Wien

calculation shows that maximum radiation emitted by an ice target occurs in the spectral region 9.89 μm to 11.45 μm. Solar reflectance or scattering is not a factor in this region and radiative power depends upon the thermal properties of the target only. Calculations using Planck's curves also shows that the spectral region around 10 μm is prime for infrared ice hazard detection. The Planck calculations and the Stefan-Boltzmann calculations link the three together showing that the radiant exitances are in agreement. The GEN-15-C Radiation Calculator acts as an independent check on the calculations using the laws. It can be seen from these calculations that the spectral region around 10.6 μm appears to be the prime spectral region for detecting targets and backgrounds that have ambient temperature values.

Both the Radiation Calculator and calculations from radiation laws show that emissivity ranges of 0.7 to 1.0 can be expected for the ice targets. These values would be important in the assessment of any field data collected with infrared systems as temperature of target measured with a blackbody system would have to be multiplied by emissivity to obtain true target temperature. As the sky and ocean are close to blackbody the true value of the target

temperature will be important in determining detection on the basis of temperature. Emissivity will also be important as it is expected that irregular shaped icebergs will not be Lambertian in character. This could result in irregular temperature values even over the wavelength range used that may have to be overcome in other ways to achieve a constant representative target temperature to background temperature relationship.

Sensor technology exists that can sense either of the two regions. Quantitative systems exist for both aircraft and ship or surface platforms. Thus, it is not expected that system development would be a problem.

The weak point is the lack of information on the ice hazard targets. Sensors exist, the effects of background radiation are reasonably known and two infrared regions exist that could be utilized. The experimental data which is very sparse when used in conjunction with theoretical considerations indicates that the 8 to 14 μm region would be the better of the two regions for infrared sensing of ice hazard targets.

7.2 Recommendations

Because of the lack of data concerning the targets to be sensed a target/characterization study is required. A quantitative sensor system is required. The use of a quantitative system will provide accurate "numbers" that can be used to classify the various targets and assess how these "numbers" vary due to differing environmental factors. Once the data can be classified in this manner the "numbers" will become infrared signatures for the particular targets. These targets will then have a characteristic signature that can be used for real time operational detection.

Even though it appears the 8 to 14 μm window will be the most effective, the available quantitiative systems can operate simultaneously in both the 3 to 5 micrometer and 8 to 14 micrometer windows. Thus, parallel signatures could be achieved and a comparison made between data from the two windows. The signatures that are developed in this manner will relate to the target and its environment. These signals must also be related to sensor variables such as lens type and field of view, aperture size of the system, the type of filter used and the type of detector used. These variables can be linked by transfer functions and the combined transfer function can then be related to the

target signature. How the target signature changes with the various combined transfer functions can then be assessed to determine the optimum system configuration required for ice hazard detection using infrared sensors.

7.3 Conclusions

From this study it can be seen that the potential exists to detect ice hazards using infrared sensing systems. This can be done for both ship and airborne sensors. The means exists to develop target signatures that will be characteristic of the ice target sensed. The major requirement is the development of these characteristic target signatures and the evaluation of any proposed sensor system in terms of these signatures. Once the signatures are known any sensor system can be evaluated without extensive field measurement by using the system transfer functions.

Infrared systems can preform a vital function as part of an ice hazard detection system. When used in conjunction with radar, sonar and low light level television systems more reliable ice hazard detection should be possible.

REFERENCES

Advanced Infrared Technology - Intensive Short Course Notes, (1971) University of Michican Summer Courses in Continuing Engineering Education

Bajzak, D., (1974), "Thermal Mapping of Water Envelopes Surrounding Icebergs" Proc. of the Second Canadian Symposium on Remote Sensing, Guelph, Ontario p 573-579

Barnes Engineering Company (1970), Handbook of Non-Contract Temperature Measurement and Control for Industry

Bell, E.E., I.L. Eisner and R.A. Oetjen, (1956), "The Spectral Distribution of the Infrared Radiation from the Sky" Proc. of the Symposium on Infrared Backgrounds, Engineering Research Institute, The University of Michigan, Nonr-1224 (12), AD 121010

Bell, E.E., L. Eisner, J. Young and R.A. Oetjen, (1960), "Spectral Radiance of Sky and Terrain at Wavelengths between land 20 Microns. II. Sky Measurements", J. of the Optical Society of America, Volume 50, p 1313-1320

Bell, E.E., L. Eisner, J. Young and R.A. Oetjen, (1962), J. of the Optical Society of America, Volume 52, p 201-209

Brock, G.C., D.I. Harvey, R.J. Kohler, and E.P. Myskowski, (1965), "Photographic Considerations for Aerospace" Itek Corporation, Lexington, Mass.

Canada Centre for Remote Sensing (1977), Information Bulletin, Airborne Operations, Third Edition, Department of Energy, Mines and Resources Canada

Cox, C. and W. Munk, (1956), Bulletin of the Scripps Institution of Oceanography, University of California Volume 6, p 401-488

Ewing, G.C. and E.D. McAlister ,(1960), Science, Volume 131, May 6, p 1374-1376

Ewing, G.C., (1965), "Oceanography from Space" Woods Hole Oceanographic Institution, Woods Hole, MA, WHOI Ref. No. 65-10

Gates, D.M., (1966), "Spectral Distribution of Solar Radiation at the Earth's Surface" Science, American Association for the Advancement of Science, Washington, D.C., Volume 151, p 523

Gordon, J. and P. Church, (1966), "Overcast Sky Luminances and Directional Luminous Reflectances of Objects and Backgrounds under Overcast Skies", Applied Optics, Volume 5, 919

Handbook of Military Infrared Technology (1965), Office of Naval Research, U.S. Navey, 906 pages

Harrison, A.W. and A.V. Jones, (1957), J. of Atmospheric and Terrestrial Physics, Pergamon Press, New York, N.Y., Volume 11, p 192-199

Idso, S.B. and R.D. Jackson (1969) "Thermal Radiation from the Atmosphere" J. of Geophysical Research, A.G.U., Washington, D.C., Volume 74, page 5397.

Infrared Technology - Intensive Short Course Notes, University of Michigan, (1971)

Infrared Handbook (1978), The Infrared Information and Analysis (IRIA) Centre, Environmental Research Institute of Michigan

Jenkins and White, (1957), Fundamentals of Optics, McGraw-Hill Book Company, New York, 637 pages

Ketchen, H.G., P.E. La Violette and R.D. Worsfold (1977) "Thermal Studies of the Grand Banks Gulf Stream Slope Using Airborne Radiation Thermometers and Satellite Data" Proc. of the Fourth Canadian Symposium on Remote Sensing, Quebec City, P.Q., p 163-179

Manual of Remote Sensing, Volume I and II, (1975), American Society of Photogrammetry, 2144 pages

McMahon, H.O., (1950), "Thermal Radiation from Partially Transparent Reflecting Bodies" J. of Optical Society of America, Volume 40, p 376-380

Moon, P., (1940) J. of the Franklin Institute, Volume 230, No. 40

Mueller, F., H. Blatter and G. Kappenburger, (1975), "Temperature Measurement of Ice and Water Surfaces in the North Water Area Using an Airborne Radiation Thermometer" J. of Glaceology, Volume 15, No. 73, p 241-250

O'Brien, H.W. et al, (1975), "Red and Near Infrared Spectral Reflectance of Snow", U.S. Army Cold Region Research and Engineering Labratory, Hanover, N.H.

Parashar, S., C. Gosselin, G. Stapleton, R. Worsfold, and R. Stacey, (1981), "Shorebased Radar Ice Measurements from Bylot Island" Presented at Oceans 81, Boston, Mass.

RCA Elctro-Optics Handbook, Technical Series EOH-11, Lancaster, Penn.

Remotec Applications Inc., (1980), Evaluation and Development of a Ship-mounted Ice Hazard Detection System, Phase I, 1980

Stair, Jr., A.T., J.C. Ulwick, K.D. Baker and D.J. Baker, (1975), "Rocketborne Observations of Atmospheric Infrared Emissions in the Auroral Regions" Atmospheres of Earths and Planets, Reidel Publishing Co., Boston, M.A., p 335-346

Taylor, J.H. and H.W. Yates, (1975), "Atmospheric Transmission in Infrared" J. of the Optical Society of America, Washington, D.C., Volume 47, No. 3, p 223-226

Thekakara, M.P., (1972) "Evaluating the Light from the Sun "Optical Spectra, Optical Publishing, Pittsfield, M.A., Volume 6, No. 3, p 32-35

Vestine, E.H., (1944), "Terrestrial Magnetism" J. of Geophysical Research, Volume 49, p 77-102

Wedler, E. and Richard D. Worsfold, (1979) "A Comparison of Atmospheric Correction Methods Used In Airborne Sea Surface Temperature Mapping" In Proc. of ASP-ACSM Convention, Washington, D.C., 22 pages.

Worsfold, R.D., D. Strong, H. Pike, S. Richter, and R. Ricketts, (1977), "Remote Sensing Studies; Forteau Bay, Labrador", C-CORE Report 77-1, 83 pages

Worsfold, R.D., D. Strong, B. Roberts and S. Richter, (1977), "Thermal Infrared Measurements and Error Correction Methods, Grand Banks, Newfoundland", C-CORE Report 77-2, 82 pages.

Worsfold, R.D and J. Sparkes, (1977) "Airborne Radiation Thermometer Studies and Error Correction Methods, Forteau Bay, Labrador", C-CORE Report 77-3, 66 pages

Worsfold, R.D. and D. Strong, (1977), "Thermal Infrared Studies, Forteau Bay, Labrador" Remote Sensing of Earth Resources, Volume VI, University of Tennessee, p 171-187

Worsfold, R.D., S. Parashar, R.O. Ramseier, H. Steltner, (1979) "Shorebased Radar Data for Navigation of Coastal Restricted Ice Covered Areas with Specific Examples of Bylot Island, N.W.T., Canada" In Proc. of Fifth International Conference on Port and Ocean Engineering under Arctic Conditions, Volume III